Aus der Anatomischen Anstalt

Institut der Ludwig-Maximilians-Universität München

The dose-dependent bio-mineralization effect induced by radial extracorporeal shock wave therapy and the immunohistochemical detection of mammal extracellular matrix molecules in zebra mussels, studies based on a novel bio-mineralization invertebrate animal model

Dissertation

zum Erwerb des Doktorgrades der Humanbiologie

an der Medizinischen Fakultät der

Ludwig-Maximilians-Universität München

vorgelegt von

Wenkai Wu

aus

Shandong, China

Jahr

2022

Mit Genehmigung der Medizinischen Fakultät der

Ludwig-Maximilians-Universität zu München

Erster Gutachter:	*Prof. Dr. Christoph Schmitz*
Zweiter Gutachter:	Prof. Dr. Stefan Milz
Dritter Gutachter:	PD Dr. Attila Aszodi

Dekan:	Prof. Dr. med. Thomas Gudermann

Tag der mündlichen Prüfung:	09.11.2022

Affidavit

Affidavit

Wu, Wenkai

Surname, first name

Street

Zip code, town, country

I hereby declare, that the submitted thesis entitled:

The dose-dependent bio-mineralization effect induced by radial extracorporeal shock wave therapy and the immuno-histochemical detection of mammal extracellular matrix molecules in zebra mussels, studies based on a novel bio-mineralization invertebrate animal model

is my own work. I have only used the sources indicated and have not made unauthorised use of services of a third party. Where the work of others has been quoted or reproduced, the source is always given.

I further declare that the submitted thesis or parts thereof have not been presented as part of an examination degree to any other university.

Munich, 20.05.2022 — Wenkai Wu

place, date — Signature doctoral candidate

Table of content

Affidavit **3**

Table of content **4**

List of abbreviations **5**

List of publications **6**

Your contribution to the publications **7**

2. Introduction **8**

2.1 The invertebrate animal model of zebra mussel in biomineralization and shock wave research 8

2.2 The extracorporeal shock wave therapy and bone fracture nonunions 9

2.2.1 The mechanisms of bioeffects induced by extracorporeal shock wave therapies 9

2.2.2 Clinical applications of extracorporeal shock wave therapies on bone fracture nonunions 11

2.3 The extracellular matrix molecules and biomineralization 13

2.3.1 Collagens 14

2.3.2 Proteoglycans/Glycosaminoglycans 14

2.3.3 Glycoproteins 15

2.3.4 The detection of extracellular matrix molecules in zebra mussels 15

2.4 Aim of the thesis 17

3. Results (published articles) **19**

3.1 Paper I 19

3.2 Paper II 28

4. Discussion **43**

4.1 New shell mineralization induced by radial extracorporeal shock waves in zebra mussels 43

4.1.1 Radial extracorporeal shock waves can induce biomineralization in the shell 43

4.1.2 The shell biomineralization induced by radial extracorporeal shock waves has a dose-effect relationship 44

4.2 The immunodetection of extracellular matrix components in zebra mussel soft tissues 46

4.2.1 Collagen IV, fibronectin, keratan sulfate (MZ15 - epitope) in zebra mussel hemocytes 46

4.2.2 Collagen IV in the peripheral nervous system 48

4.2.3 Aggrecan and link protein in the byssus glands 48

4.2.4 Other extracellular matrix molecules located in the zebra mussel soft tissues 50

5. Summary **52**

6. Zusammenfassung **54**

7. References **56**

Acknowledgements **63**

List of abbreviations

BMP-2: Bone morphogenetic protein 2

COL1A1: Collagen type I alpha 1 chain

Ca2+: Calcium ions

DKK-1: Dickkopf related protein 1

eNOS: Endothelial nitric oxide synthase

ECM: Extracellular matrix

EFD: Energy flux density

ERK: Extracellular signal-regulated kinases

ESW: Extracorporeal shock wave

rESW: Radial extracorporeal shock wave

fESW: Focused extracorporeal shock wave

ESWL: Extracorporeal shock wave lithotripsy

ESWT: Extracorporeal shock wave therapy

rESWT: Radial extracorporeal shock wave therapy

fESWT: Focused extracorporeal shock wave therapy

FAK: Focal adhesion kinase

GAG: Glycosaminoglycan

IGF-1: Insulin-like growth factor 1

PCNA: Proliferating cell nuclear antigen

PG: Proteoglycan

RUNX2: Runt-related transcription factor 2

SPARC: Secreted protein, acidic and rich in cysteine

SMPs: Shell matrix proteins

TGF-β1: Transforming growth factor-beta1

TLR3: Toll-like receptor 3

VEGF: Vascular endothelial growth factor

vWF: von Willebrand factor

List of publications

This thesis is based on the following publications

I. **Exposure of zebra mussels to radial extracorporeal shock waves: implications for treatment of fracture nonunions.**
Wenkai Wu, Nicola Maffulli, John P. Furia, Lukas Meindlhumer, Katharina Sternecker , Stefan Milz, Christoph Schmitz.
Journal of Orthopaedic Surgery and Research. 2021 Dec 4;16(1):707. doi:10.1186/s13018-021-02852-1.

II. **Immunohistochemical Detection of Various Proteoglycans in the Extracellular Matrix of Zebra Mussels.**
Wenkai Wu, Juergen Geist, Sebastian Beggel, Christoph Schmitz, Stefan Milz, Katharina Sternecker.
Fishes. 2022 Mar 24; 7(2): 74. https://doi.org/10.3390/fishes7020074

Your contribution to the publications

1.1 Contribution to paper I

This study was designed by Christoph Schmitz and Katharina Sternecker. Lukas Meindlhumer and I carried out all the experiments, including the mussel incubation, measurement, and selection, the exposure of mussels to radial shock waves, the incubation of mussels in calcein solution, the sacrifice of mussels, the mussel shell embedding, the mussel shell MMA blocks sectioning and grinding. I measured the fluorescence intensity, organized the data, and did the statistical analysis with Christoph Schmitz and Katharina Sternecker. I drew sketches, arranged the figures, and wrote the manuscript. Christoph Schmitz, Katharina Sternecker, Stefan Milz, Nicola Maffulli, and John P. Furia reviewed and revised the manuscript.

1.2 Contribution to paper II

This study was designed by Christoph Schmitz, Stefan Milz, and Katharina Sternecker. I carried out all experiments, including the immunohistochemical staining, the production of mussel soft body paraffin sections, and the identification of mussel soft body anatomical structures. I organized the data and interpreted the results with Stefan Milz. I drew sketches, arranged the figures, and wrote the manuscript. Christoph Schmitz, Stefan Milz, Katharina Sternecker, Sebastian Beggel and Juergen Geist reviewed and revised the manuscript.

2. Introduction

2.1 The invertebrate animal model of zebra mussel in biomineralization and shock wave research

Mollusks are widespread invertebrate animals distributed in marine, freshwater, and certain areas of land. Bivalves are the second-largest division of the mollusk phylum [1] and have been closely associated with human life since ancient times. In scientific research, bivalves have always been an important point of interest in bionics, evolutionary biology, ecotoxicology, and other fields [2-4]. In ecotoxicology and environmental sciences, bivalve mussels play an essential role in water purification and pollution monitoring [5-8]. In bionics, the formation of shells and byssus in bivalves have been important topics for the studies of biological mineralization and adhesion processes in animals [3, 9-11]. Although the shell mineralization in bivalves has been a research hotspot recently, the mussel animal model has been seldomly used in biomedical studies [12].

Most biomedical research was conducted using vertebrate animals such as mice, rats, and rabbits. While the 3Rs principles (Replacement, Reduction, and Refinement) have been calling as ethical guiding principles with the aim to reduce animal experiments as low as possible and to replace animal experiments with other alternatives. In particular, the mussel as a widespread invertebrate could be an excellent alternative experimental invertebrate animal in specific fields of research.

In a previous study, the zebra mussel was used as a biomineralization animal model to study the new biomineralization induced by extracorporeal shock waves (ESWs) [12]. The freshwater environment surrounding the shell makes a perfect propagation medium for shock waves. The acoustic investigation of shock wave energy flux density (EFD) distribution in water makes a vital foundation for studying the dose-effect relationship between the shock wave energy level and the induced biomineralization effect in animals [12-14]. Furthermore, studies of the soft tissue extracellular matrix (ECM) molecules might bring us pieces of evidence to explain the internal biomineralization process in mussels. Therefore, two projects were arranged to research the dose-dependent biomineralization effects

after radial extracorporeal shock wave therapy (rESWT) and the immunohistochemical detection of ECM molecules in zebra mussels.

2.2 The extracorporeal shock wave therapy and bone fracture nonunions

2.2.1 The mechanisms of bioeffects induced by extracorporeal shock wave therapies

The shock wave is a kind of discontinuous peak propagation in a medium such as air, water, or even a solid substance. When it encounters obstacles in the transmission route, the shock wave can cause a pressure change on the interface between two kinds of materials with high positive pressure up to 100 MPa and negative pressures of 5-10 MPa within 10 μs (Figure 1) [15-17]. Rapid pressure change caused not only tensile and shearing forces but also another phenomenon called cavitation in the medium. Cavitation is the formation of some small cavities in places where the pressure is relatively low. When exposed to higher pressure, these small cavities or bubbles collapse and create a strong shock wave close to the bubbles [18]. With those side effects, shock waves can cause damage to artificial objects such as control valves, pumps, propellers, and impellers. However, as more research focuses on shock waves, we gradually become able to minimize the harm and take advantage of its strengths in many fields.

In the biomedical field, the mechanism of the biological effects of ESWs in living tissues remains uncertain. However, studies on ESWs revealed many biological reactions, which could be concluded mainly in two phases. In the physical phase, the tensile and shearing forces caused by ESWs on cell membranes and ECM might increase the permeability of cell membranes by stretching sensitive ion channels or change the biochemical activity of enzymes and proteins by changes in structures [19]. Subsequently, many signal transduction pathways (FAK, ERK, TLR3) were activated to modulate certain gene expressions [20-26].

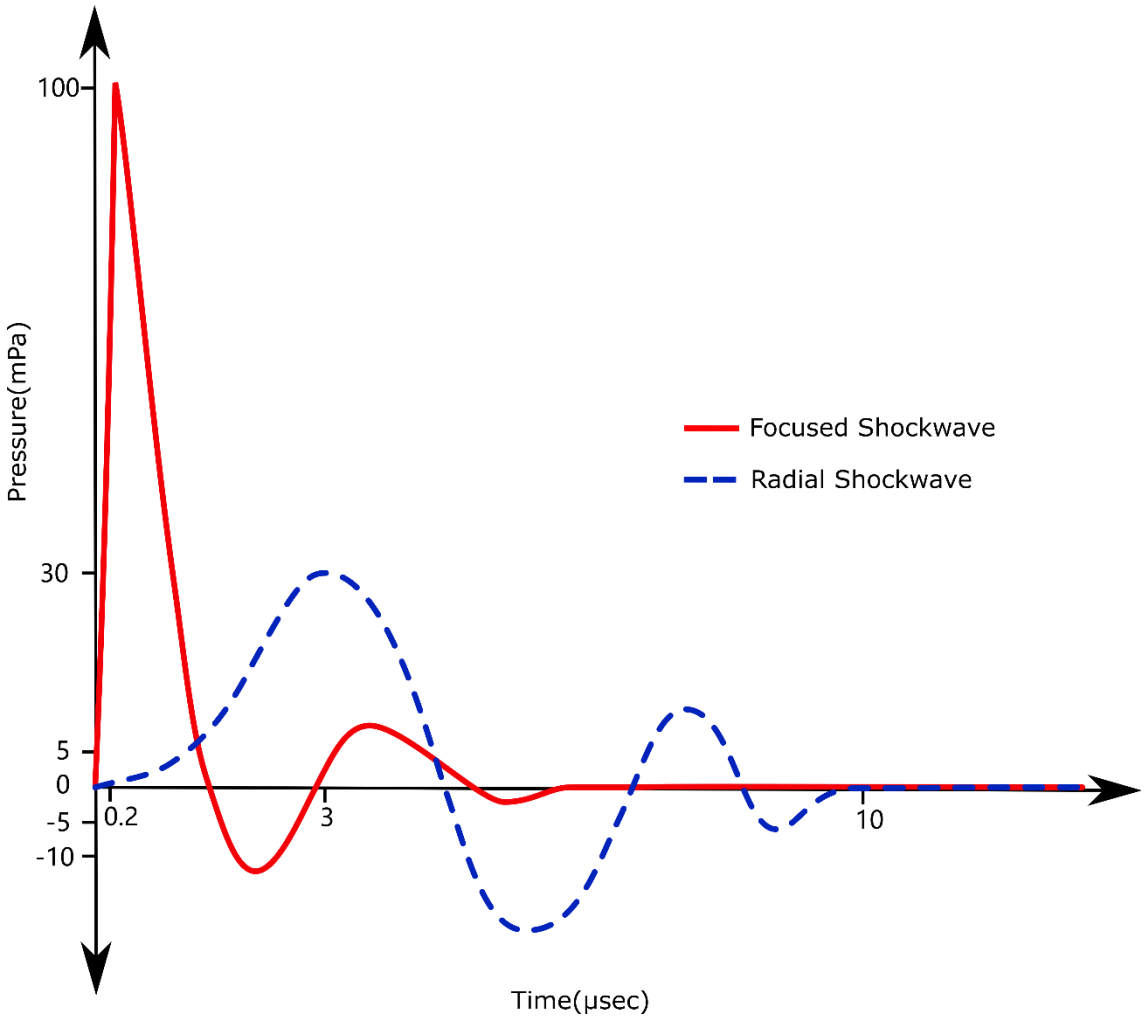

Figure 1. A schematic pressure profile of focused and radial extracorporeal shock waves (fESWs and rESWs). The fESWs can cause much greater pressure changes than rESWs. Modified from Salter et al., 2020 [16] and the "Physical Principles of ESWT: Basic Physical Principles." The International Society for Medical Shockwave Treatment. https://www.shockwavetherapy.org/about-eswt/physical-principles-of-eswt/ [17].

In the biological phase, molecular biology studies have also shown that ESWT can up-regulate the expression of key biomolecules for angiogenesis (vWF, VEGF, eNOS, and PCNA) and osteogenesis (BMP-2, osteocalcin, alkaline phosphatase, DKK-1, and IGF-1) at the gene or molecular level, which could induce bone formation directly or indirectly [21, 26-30].

According to present studies, the mechanism of ESWT promoting bone formation/healing may be initiated in the following ways, 1) ESWT could promote neovascularization and bone healing with the enhancement of angiogenesis and

osteogenesis growth factors (including eNOS, VEGF, PCNA, and BMP-2) [29], 2) ESWT induces the elevation of nitric oxide, osteocalcin, and transforming growth factor-beta1 (TGF-β1) and then enhanced the proliferation and differentiation of osteoblasts [31], 3) the mechanical stimulus of ESWT promotes biological bone healing processes through mechanotransduction [32], 4) ESWT induces the gene expression of ECM proteins (COL1A1, osteocalcin, and osteopontin) [33], 5) rESWs significantly promoted the proliferation and self-renewal of MSCs [34].

2.2.2 Clinical applications of extracorporeal shock wave therapies on bone fracture nonunions

The clinical use of the shock wave as a kind of physical treatment was named extracorporeal shock wave therapy (ESWT). The initial clinical use of ESWT was introduced in urologic stones in 1982 [35]. Because of its noninvasiveness and effectiveness, it was quickly and widely popularized. The extracorporeal shock wave lithotripsy (ESWL) has become the first choice to treat kidney and ureteral stones. In addition to the ESWL, shock waves have also been found to promote osteogenesis as a side effect in ESWL-treated patients [36]. Early in 1991, the ESWT was used in the treatment of delayed and non-union of fractures with a remarkable effective rate [37]. Since then, more and more attempts of ESWTs had been put into practice on many musculoskeletal disorders. In addition to the bone fracture nonunion, the ESWT is also effective in treating many chronic tendinopathies and wound healings. To date, the average union rate after ESWT in delayed unions was 86%, in nonunions was 73%, and in nonunions after surgical treatment was 81% [38]. Although the ESWT showed similar effectiveness as the surgical treatments with a much lower rate of complication, in clinical situations, the surgical treatment is still the “golden standard” treatment for fracture nonunions or delayed unions because of its high union rate (74%-95%) [39-41].

In the clinical application of ESWT, two kinds of extracorporeal shock wave devices (the radial and focused extracorporeal shock wave equipment) have been developed respectively for the treatment of superficial and deep lesions. As summarized in the literature, most medical institutes tend to use the fESWT to treat nonunion fracture patients because of the higher energy and deeper effective area of fESWs (penetration depth rESWT 20mm, fESWT 95mm, Figure 2) [13, 42]. This choice was supported by a previous animal experiment in which a

threshold energy level of fESWT was found to be essential for initiating new bone formation [43].

Figure 2. Comparison of penetration depth of focused and radial ESWT devices

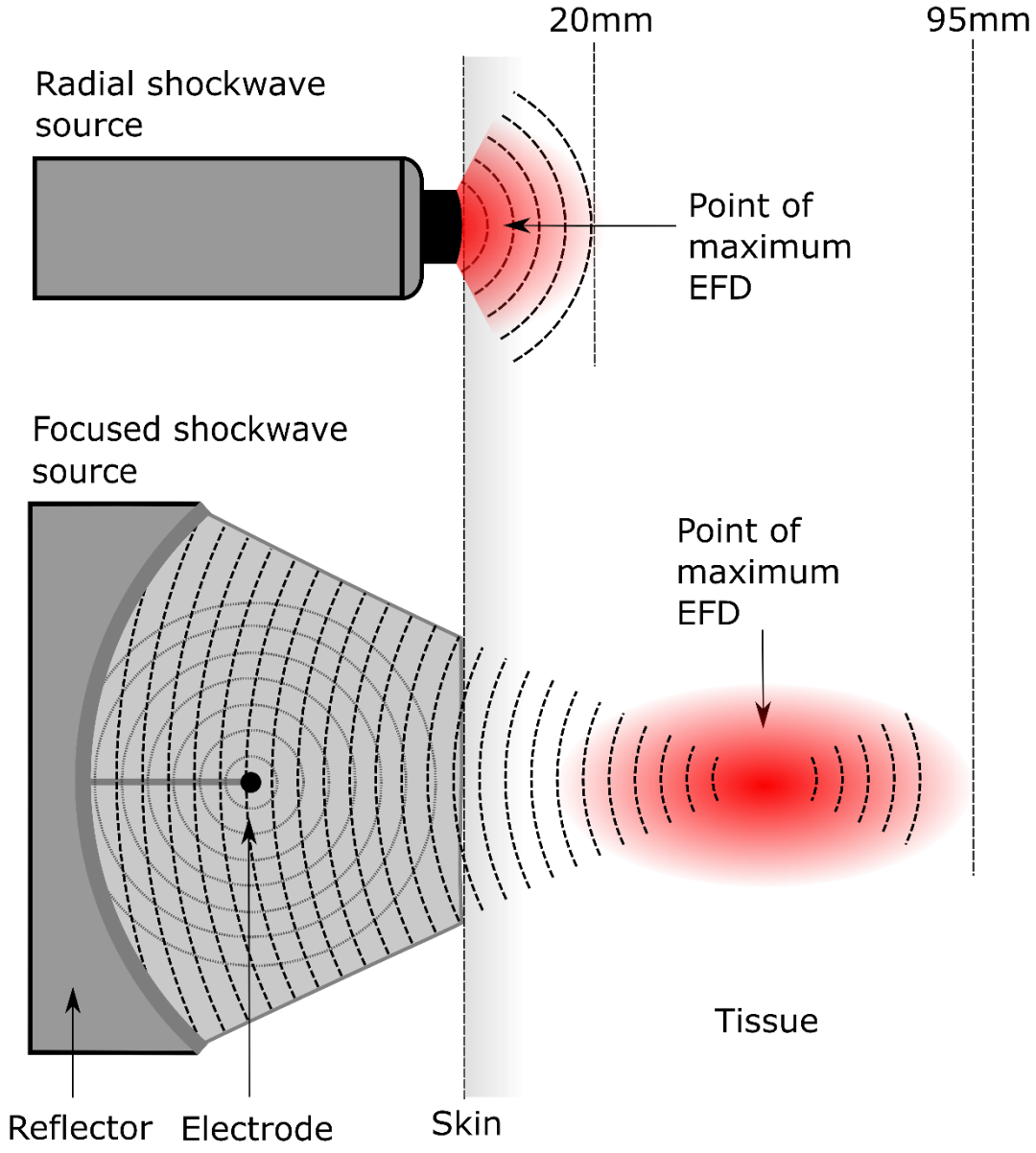

The penetration depth of fESWs is deeper than that of rESWs, data measured in water using rESWT and fESWT devices (Swiss DolorClast and Swiss Piezoclast; Electro Medical Systems, Nyon, Switzerland) [13]. Modified from the “Physical Principles of ESWT: Basic Physical Principles.” The International Society for Medical Shockwave Treatment. https://www.shockwavetherapy.org/about-eswt/physical-principles-of-eswt/ [17].

While with the development of radial shock wave techniques, the radial shock wave devices are currently more portable and easy to operate than the focused shock wave devices. Some doctors chose to try rESWs to treat superficial bone fracture delayed unions or nonunions with a remarkable outcome in patients with tibia fracture (union rate of 70% in tibia nonunions) and other superficial bone fractures in hand and foot [42]. This raises the possibility that the rESWT might be more suitable for superficial bone fracture nonunion patients.

For a long time, the radial shock wave was considered a kind of mechanical wave (generated by hitting the metal applicator with an accelerated projectile) because of its different principle of generation from the focused shock wave devices (Electrohydraulic/Electromagnetic/Piezoelectric sources). This concept was not updated until the observation of the cavitation phenomenon in rESWT studies [14]. Research of rESWT in animals also demonstrated significant bioeffects of new bone formation in vivo induced by the rESWs [44-46]. Results of all those studies have led us to a hypothesis that the rESWs might have similar bioeffects just as the fESWs.

Besides, the osteogenesis-promoting effects of low energy rESWs raise the question: Is the high energy level necessary for the ESW-induced biomineralization? Although the rESWT is relatively low in energy density (maximum EFD 0.14 mJ/mm2 with the nearest distance of 1mm) [14], the clinical applications of ESWT in bone fracture nonunions also differ a lot in energy densities (from 0.09 to 1.10 mJ/mm2) [38]. More experiments are required to investigate the relationship between the energy density and bioeffects of rESWT. Here we used an invertebrate zebra mussel animal model to explore the relationship between the new mineralization intensity in the shell and the energy level of rESWs.

2.3 The extracellular matrix molecules and biomineralization

The ECM is a non-cellular network composed of a series of macromolecules present in all tissues of multicellular organisms. The network lies outside a cell but is made and maintained by a cell. The ECM provides not only essential physical scaffolding that supports the tissue but also plays a crucial role in cell adhesion, tissue morphogenesis, and differentiation [47-49]. The extracellular molecules

consist of collagens, glycosaminoglycans, proteoglycans, and many glycoproteins. Minerals and enzymes also present as components in some specific tissues. Although most ECM studies have focused on vertebrate species, the studies of the ECM in invertebrates are important in revealing the origins of ECM in evolution [50, 51]. To achieve this, some human ECM molecules related to osteogenesis were selected, including collagens, proteoglycans/glycosaminoglycans, and glycoproteins.

2.3.1 Collagens

Collagen is the most abundant protein in mammals acting as the main structural protein in the ECM of various connective tissues. The triple helix structure and the inter/intra-chain crosslinks of collagen are crucial to its mechanical properties [52, 53]. In the family of collagens, type I collagen constitutes the largest proportion (over 90%) of collagens. It plays as the main component of the organic part of the bone. Type II collagen acts as the main collagenous component of cartilage. Type III collagen is the main component of reticular fibers, usually found alongside type I collagen. Type IV collagen is the main component of basal lamina in various tissues. The primary function of collagenous proteins is to provide mechanical support to tissues and allow biochemical interaction.

2.3.2 Proteoglycans/Glycosaminoglycans

Proteoglycans are heavily glycosylated proteins that are also major components of the human and animal ECM. They work together with other proteoglycans, hyaluronic acids, and fibrous matrix proteins such as collagen. They form large complexes that fill the intercellular spaces. Proteoglycans consist of a core protein and one or more glycosaminoglycan (GAG) chains linked by covalent bonds. The GAG residues found in proteoglycans are heparan sulfate, chondroitin sulfate, keratan sulfate, hyaluronic acid, and dermatan sulfate [54]. Other than acting as intercellular substances, proteoglycans may also be involved in regulating cell adhesion, cell growth, proliferation, angiogenesis, tumor metastasis, or other biological activities. Aggrecan is the major proteoglycan in the articular cartilage that provides the cartilage load-bearing properties via interaction with hyaluronan and link protein. Besides, a dermatan sulfate proteoglycan extracted from the

eggshell matrix had shown a concentration-dependent crystal morphology regulation function in vitro [55].

2.3.3 Glycoproteins

Glycoproteins such as osteonectin, osteopontin, alkaline phosphatase, fibronectin, and fibrillin are produced in different stages of skeletal development and bone remodeling with various functions related to cell attachment and migration, cell-matrix interactions, bone mineralization, and pathological process such as bone metastasis. The osteonectin (SPARC), as a regulator of calcium release, may participate in the collagen mineralization process by binding with collagen and hydroxyapatite crystals [56]. The osteopontin in bone could stimulate the migration and adhesion of osteoclasts and the proliferation and calcification of osteoblasts [57]. Fibronectin was indispensable in the initial steps of collagen polymerization, and it can regulate the differentiation of osteoblast by cell-fibronectin interaction [58].

2.3.4 The detection of extracellular matrix molecules in zebra mussels

The research of ECM in mollusks could be divided into two aspects, the shell matrix and the ECM in soft tissues. Studies of the shell matrix components mainly focused on the mechanism of shell formation. There are mainly two hypotheses of shell formation mechanisms, the traditional matrix-mediated hypothesis and the new cell-mediated hypothesis of shell formation. The traditional matrix-mediated hypothesis states that the shell formation is initiated from solution by the extracellular organic matrix [59]. This hypothesis was mainly supported by experiments in which the extractions of shell matrix showed abilities to induce crystal formation in vitro [60, 61]. The cell-mediated hypothesis was brought up along with the report of a class of granulocytes that contain calcium carbonate crystals in Oysters [62]. This hypothesis was supported by subsequent studies, which demonstrated the presence of crystal-bearing granulocytes in the extrapallial space and the calcium carbonate mineralization mediated by mantle cells [63, 64]. To date, the cell-mediated shell formation theory was composed of two parts, the formation of calcium carbonate crystals associated with mantle cells and the crystal deposition from intracellular calcium carbonate to the mineralization site, which was mediated by hemocytes (Figure 3) [11]. In both hypotheses of shell

biomineralization, the mussel soft tissues were involved in biology mineralization or crystal deposition.

Most detections of mussel soft tissue ECM components were conducted by genomics studies [65]. The ECM compositions in mussels can be screened and identified by analyzing gene expression data. An immunohistochemical study aimed at the immunolocalization of shell matrix proteins (SMPs) in soft tissues showed the existence of SMPs in hemolymph, heart, gill, mantle, and adductor muscle tissues [66]. Another study has identified the biomineralization-related proteins and localized the selected gene transcripts in regions of mantle tissues by in situ hybridization [67].

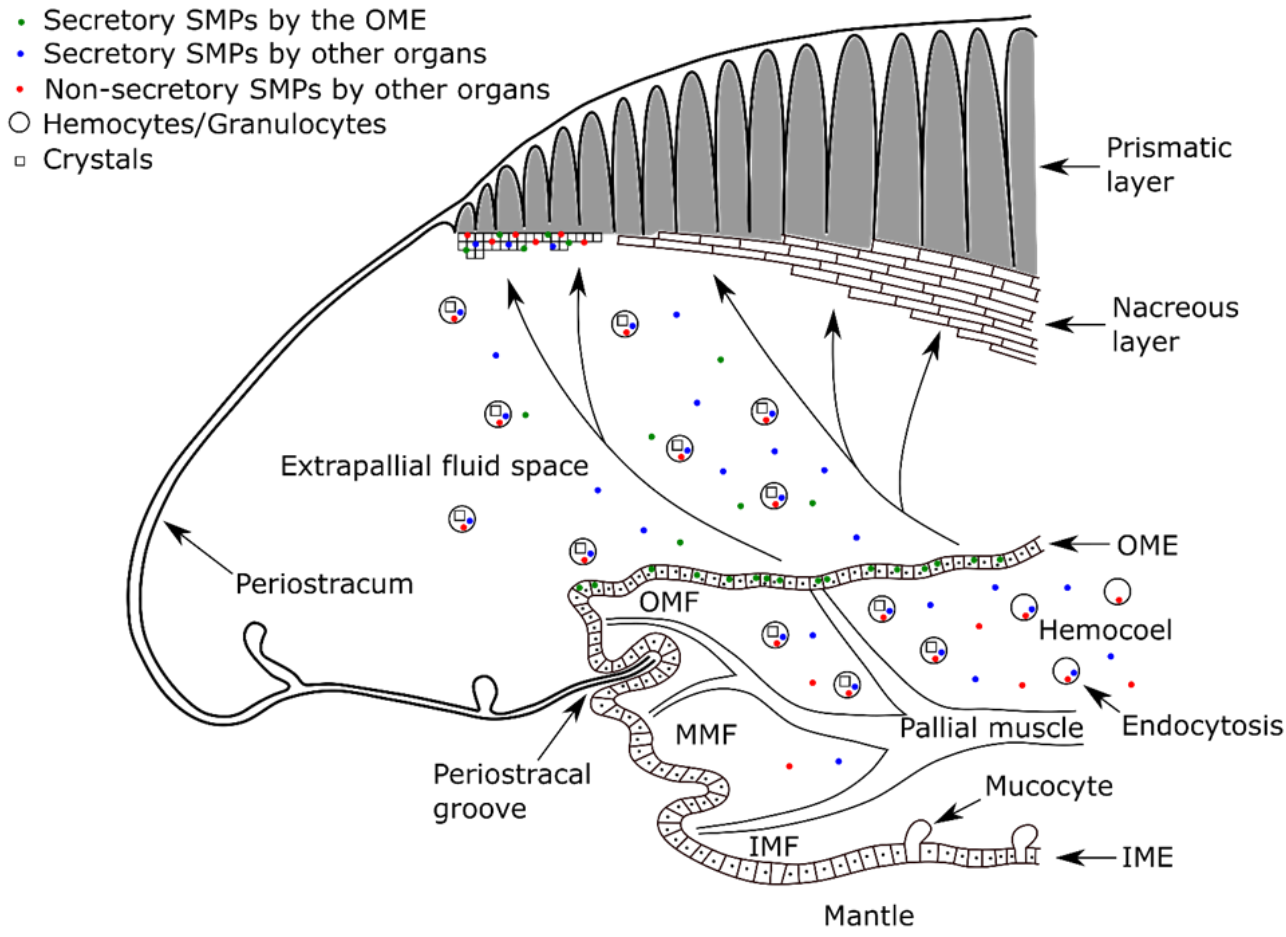

Figure 3. Schematic presentation of shell biomineralization

The figure includes mainly two parts: the soft body and the shell. Crystal-bearing hemocytes in the circulatory system are released into the extrapallial fluid through secretory cavities on the mantle surface. These hemocytes participate in the formation of the prismatic layer by fusing into the prismatic layer columns and releasing calcium carbonate crystals to form the calcite. Besides, hemocytes

(mainly granulocytes) also transport non-secretory shell matrix proteins (SMPs) by endocytosis in soft bodies and releasing them in the biomineralization front. SMPs: Shell matrix proteins; OMF: outer mantle fold; MMF: middle mantle fold; IMF: inner mantle fold; OME: outer mantle epithelium; IME: inner mantle epithelium. The involvement of hemocytes in the nacreous layer formation remains a point of concern. Modified according to Böhm et al., 2019 [10] and Song et al., 2019 [11].

Although numerous studies have reported those shell mineralization-related genes and proteins in mussels, the functions of these proteins and genes remain unknown. It is noteworthy that mineralized genes and proteins have been reported to be conserved [67]. Here we focused on the immunodetection of mammal ECM molecules in zebra mussel soft tissues trying to find connections between human and mussel biomineralization.

2.4 Aim of the thesis

The ESWT is a promising non-invasive physical therapy for nonunions and delayed unions, with excellent union rates. The application of ESWT on bone nonunions could reduce the financial costs and physical trauma for patients. However, the principles of radial and focused ESWTs remain unknown, and clinical applications of ESWT are still lacking explicit guidelines. Here we used the zebra mussel as a novel biomineralization animal model to explore the relationship between the energy of rESWs and the rESW-induced biomineralization. The mechanism of shell mineralization in mussels has been a hot topic in biomineralization research. Research on the shell mineralization mechanisms in invertebrate animals could improve our understanding of the biological mineralization process in the early stage of evolution. The ECM is vital for the development of tissues and organs in multicellular organisms. With no specific organs and structures responsible for the mineralization, the study of the ECM molecules might be a good point of interest to investigate the shell biomineralization mechanisms in mussels. A series of monoclonal antibodies of mammal ECM molecules (some of them related to biomineralization) were selected for the immunohistochemical study on the soft tissue of zebra mussels.

In this thesis, our ultimate goal is to further understand the mechanisms of the rESW-induced biomineralization process in zebra mussels. A prospective biomineralization process might be revealed, which was initiated by rESWT stimulation, mediated by the biological activities in cells and ECM, and ended up in the shell mineralization.

To explore the biophysical processes, we aimed to investigate the following topics.

1. Whether the rESWT has the same ability to induce biomineralization in zebra mussels as the fESWT.
2. The relationship between the shell biomineralization intensity and the energy level of rESWT on mussels.
3. The presence of mammal ECM molecules in zebra mussel soft tissues.
4. The potential functions of mammal ECM molecules in zebra mussel tissues.

3. Results (published articles)

3.1 Paper I

Wu *et al.*
Journal of Orthopaedic Surgery and Research (2021) 16:707
https://doi.org/10.1186/s13018-021-02852-1

Journal of Orthopaedic Surgery and Research

RESEARCH ARTICLE Open Access

Exposure of zebra mussels to radial extracorporeal shock waves: implications for treatment of fracture nonunions

Wenkai Wu[1], Nicola Maffulli[2,3,4], John P. Furia[5*], Lukas Meindlhumer[1], Katharina Sternecker[1], Stefan Milz[1] and Christoph Schmitz[1]

Abstract

Background: Radial extracorporeal shock wave therapy (rESWT) is an attractive, non-invasive therapy option to manage fracture nonunions of superficial bones, with a reported success rate of approximately 75%. Using zebra mussels (*Dreissena polymorpha*), we recently demonstrated that induction of biomineralization after exposure to focused extracorporeal shock waves (fESWs) is not restricted to the region of direct energy transfer into calcified tissue. This study tested the hypothesis that radial extracorporeal shock waves (rESWs) also induce biomineralization in regions not directly exposed to the shock wave energy in zebra mussels.

Methods: Zebra mussels were exposed on the left valve to 1000 rESWs at different air pressure (between 0 and 4 bar), followed by incubation in calcein solution for 24 h. Biomineralization was evaluated by investigating the fluorescence signal intensity found on sections of the left and right valves prepared two weeks after exposure.

Results: General linear model analysis demonstrated statistically significant ($p < 0.05$) effects of the applied shock wave energy as well as of the side (left/exposed vs. right/unexposed) and the investigated region of the valve (at the position of exposure vs. positions at a distance to the exposure) on the mean fluorescence signal intensity values, as well as statistically significant combined energy × region and energy × side × region effects. The highest mean fluorescence signal intensity value was found next to the umbo, i.e., not at the position of direct exposure to rESWs.

Conclusions: As in the application of fESWs, induction of biomineralization by exposure to rESWs may not be restricted to the region of direct energy transfer into calcified tissue. Furthermore, the results of this study may contribute to better understand why the application of higher energy flux densities beyond a certain threshold does not necessarily lead to higher success rates when treating fracture nonunions with extracorporeal shock wave therapy.

Keywords: rESWT, Biomineralization, Mussel shell, Calcein green, Fracture non-union

Background

Extracorporeal shock wave therapy (ESWT) has become an attractive, non-invasive option for the management of fracture nonunions [1–3]. Current treatment protocols recommend exact application of focused extracorporeal shock waves (fESWs) at the fracture line with the highest possible energy flux density (EFD) [4, 5]. This requires high effort and large, stationary and expensive focused ESWT (fESWT) devices. On the other hand, recent

*Correspondence: jfuria@ptd.net
[5] SUN Orthopedics of Evangelical Community Hospital, 210 JPM Rd, Lewisburg, PA 17837, USA
This paper contains data from the Ph.D. thesis of Wenkai Wu as well as the M.D. thesis of Lukas Meindlhumer.
Full list of author information is available at the end of the article

reports described successful treatment of fracture nonunions of superficial bones using radial ESWT (rESWT) [3, 6], in line with what was obtained in animal models [7, 8], with a reported success rate of approximately 75% [3, 6].

Both fESWs and radial extracorporeal shock waves (rESWs) are single acoustic impulses which have an initial high positive peak pressure between 10 and more than 100 megapascals that is reached in less than one microsecond (µs) [9, 10]. The positive pressure is followed by a low tensile amplitude of a few microseconds duration that can generate cavitation [11]. The life cycle of single fESWs or rESWs is approximately 10–20 µs [9–11]. Given these characteristics, fESWs and rESWs fundamentally differ from therapeutic ultrasound. Furthermore, fESWs differ from rESWs in terms of how the shock waves are produced, with regard to the penetration depth of the shock waves into tissue, and in terms of their physical characteristics [9, 11, 12].

Prior studies [3, 6] indicated that rESWT could become a highly attractive alternative to fESWT in the management of fracture nonunions of superficial bone (including the tibia, fibula, bones of the hand and foot, clavicle, etc.). rESWT as opposed to fESWT might be advantageous, as the former is less expensive and does not require exact application at the fracture line (and, thus, not exact positioning using, e.g., an image intensifier). Furthermore, treatment with rESWs is usually less painful than treatment with fESWs and does not require local anesthesia or sedation [12]. Further, rESWT devices are more widely used than fESWT devices, and there is no scientific evidence in favor of either rESWT or fESWT in terms of treatment outcome when treating tendon and other pathologies of the musculoskeletal system [12].

Using zebra mussels (*Dreissena polymorpha*) as a model for studying biomineralization [13], we recently demonstrated that induction of biomineralization after exposure to fESWs is not restricted to the region of direct energy transfer into calcified tissue [10] (detection of newly calcified tissue was performed by exposing the mussels to fluorescent markers that were incorporated into the shell during biomineralization). It is currently unknown whether this is also true for rESWs.

Accordingly, this study aimed to test the following hypotheses: (1) as fESWs, rESWs also induce biomineralization in zebra mussels; and (2) there is a direct dose-dependent effect in the formation of newly calcified tissue after exposure of zebra mussels to rESWs (i.e., "the more the better").

Methods

Animals

The data presented in this paper were produced in two experiments performed in 2018 ($n=60$ mussels) and 2019 ($n=30$ mussels). Zebra mussels *(Dreissena polymorpha*) were collected by hand from the rivers Götzinger Ache (Bavaria, Germany) in March 2018 and Schinderbach (Bavaria, Germany) in July 2019. The mussels were fed ad libitum with shellfish diet in 2018 and with *Chlorella vulgaris* (SAG Number 211-19; Algae collection of the University of Goettingen, Goettingen, Germany) in 2019 before and during the experiments. The mussel size was measured before sacrificing according to [14] (mean length 23 ± 2.2 mm (mean ± standard deviation); width, 12 ± 1.5 mm; height 11 ± 1.2 mm).

All experiments were performed according to German animal protection regulations which do not require registration or approval of experiments using zebra mussels.

Exposure of mussels to radial extracorporeal shock waves

The mussels were exposed to rESWs produced with a Swiss DolorClast device (Electro Medical Systems, Nyon, Switzerland), using the radial handpiece and 6-mm applicator (Figs. 1, 2a). During the first/second experiment performed in 2018/2019, $n=10/n=5$ mussels each were randomly selected and exposed to 1000 rESWs each produced using an air pressure of the rESWT device of, respectively, 0 bar (sham exposure), 2.0, 2.5, 3.0, 3.5 or 4.0 bar.

For exposure to rESWs, the mussels were fixed under water in aquarium sand (diameter 2–3 mm; Dupla Marin Reef Ground; Dohse Aquaristik, Grafschaft-Gelsdorf, Germany) to disperse and, thus, minimize the reflection of rESWs (Fig. 1). Using a drill stand, the distance between the applicator tip and the mussels was set at 2.5 mm to prevent any mechanical destruction of the mussel valve through direct contact with the applicator tip. Accordingly, the energy flux density (EFD) at 3.0 and 4.0 bar air pressure that hit the mussels was approximately 0.08 mJ/mm^2 and 0.11 mJ/mm^2 (the EFD generated using the 6 mm applicator of the handpiece of the rESWT device shown in Fig. 1 is similar to the EFD generated using the 15 mm applicator of this device [15]; the decrease in the EFD is almost linear between a distance of 1 mm and 5 mm to the applicator [15]. At a distance of 1 mm and 5 mm to the applicator, the following EFDs were measured using the 15-mm applicator [11]: 0.1 mJ/mm^2 and 0.04 mJ/mm^2 when operated at 3.0 bar air pressure, and 0.14 mJ/mm^2 and 0.06 mJ/mm^2 when operated

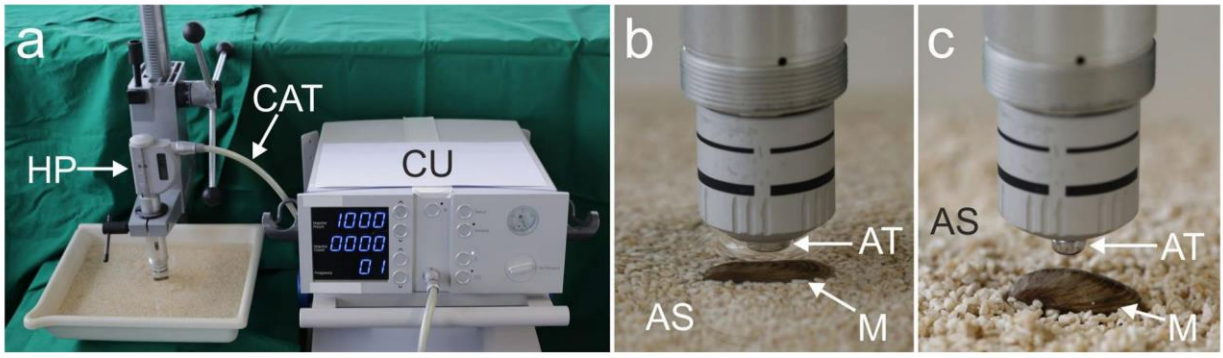

Fig. 1 Exposure of Zebra mussels to radial extracorporeal shock waves. **a** overview; **b** close-up view of the mussel and the metal applicator of the handpiece of the radial extracorporeal shock wave therapy (rESWT) device under water; **c** close-up view as in **b** but without water, showing the distance between the mussel and the applicator of the handpiece of the rESWT device. Abbreviations: CU, control unit; CAT, compressed-air tube; HP, handpiece; AT, applicator tip; M, mussel; AS, aquarium sand

at 4.0 bar air pressure). The rESWs were applied at a frequency of 8 Hz.

Immediately after exposure to rESWs or sham exposure, the mussels were incubated in calcein solution (10 mg/l; Product Number: C0875-5G; Sigma-Aldrich, St. Louis, MO, USA) for 24 h. To this end, all mussels were placed in the same aquarium which contained six liters of calcein solution, with each group of mussels in a separate glass chamber ($10 \times 15 \times 15$ cm). The position of each glass chamber within the aquarium was selected randomly. Afterwards, the mussels were housed (using the same glass chambers and aquarium) in ventilated tap water for two weeks. Then, the mussels were euthanized in 70% ethanol, and the dissected valves were dehydrated in increasing concentrations of ethanol (70%, 80% and 90% for six days each, followed by 100% for 12 days).

After fixation, both valves of each mussel were degreased in xylene for six days, followed by incubation in methanol for six days. Then, the mussel valves were embedded in methyl methacrylate (Product Number: 800590; Sigma-Aldrich) according to [16]. Polymerization took 14 days. Afterward, the polymerized methyl methacrylate blocks containing the valves (one valve per block) were cut into 400-µm-thick sections along the longest axis of the embedded valve using a ring saw microtome (SP 1600; Leica, Wetzlar, Germany) (Fig. 2b, c). The sections were ground and polished using a 400 CS micro-grinder (EXAKT Advanced Technologies, Norderstedt, Germany). The final section thickness was approximately 200 µm, measured in the middle of each section using a digimatic micrometer (Mitutoyo, Kawasaki, Japan).

Measurements of fluorescence signal intensity

Images were taken using a fluorescence microscope (Olympus BX51WI; Olympus, Tokyo, Japan) using a $4 \times$ UPlanSApo objective (numerical aperture = 0.16) (Olympus), Alexa Fluor 488 filter (49011; Chroma, Bellows Falls, VT, USA), grayscale EM CCD camera (Model C9100-02, 1000×1000 pixels; Hamamatsu Photonics, Hamamatsu City, Japan) and SOLA LED lamp (Lumencor, Beaverton, OR, USA). All images were taken with the Stereo Investigator software (64 bit, Version 11.07; MBF Bioscience, Williston, VT, USA) and saved as 8 bit TIF files (i.e., with gray values ranging from 0 to 255). Using pilot measurements, the camera was adjusted so that no image was overexposed (i.e., all gray values were smaller than 255). This resulted in the following camera settings: exposure time, 24 ms; sensitivity, 80; gamma, 1.0.

In line with our previous study [10], the strongest fluorescence signal was found over the hypostracum (Fig. 2d). Analysis of mussels after sham exposure indicated that the signal over the hypostracum was indeed caused by exposure to rESWs (Fig. 2e, f). Accordingly, measurements of fluorescence signal intensity were performed over the hypostracum, using the linear pixel plot function of the Stereo Investigator software (MBF Bioscience). Four measurement lines each (spanning 243 ± 79 µm representing 135 ± 44 pixels, depending on the curvature of the valve) were positioned over the hypostracum as shown in Fig. 2d, representing Regions A-D indicated in Fig. 2a. Region A was next to the umbo, Region D was next to the shell growth zone, and Regions B and C were in between. As in our previous study [10], the umbo itself was excluded from the analysis because of strong autofluorescence of the ligament.

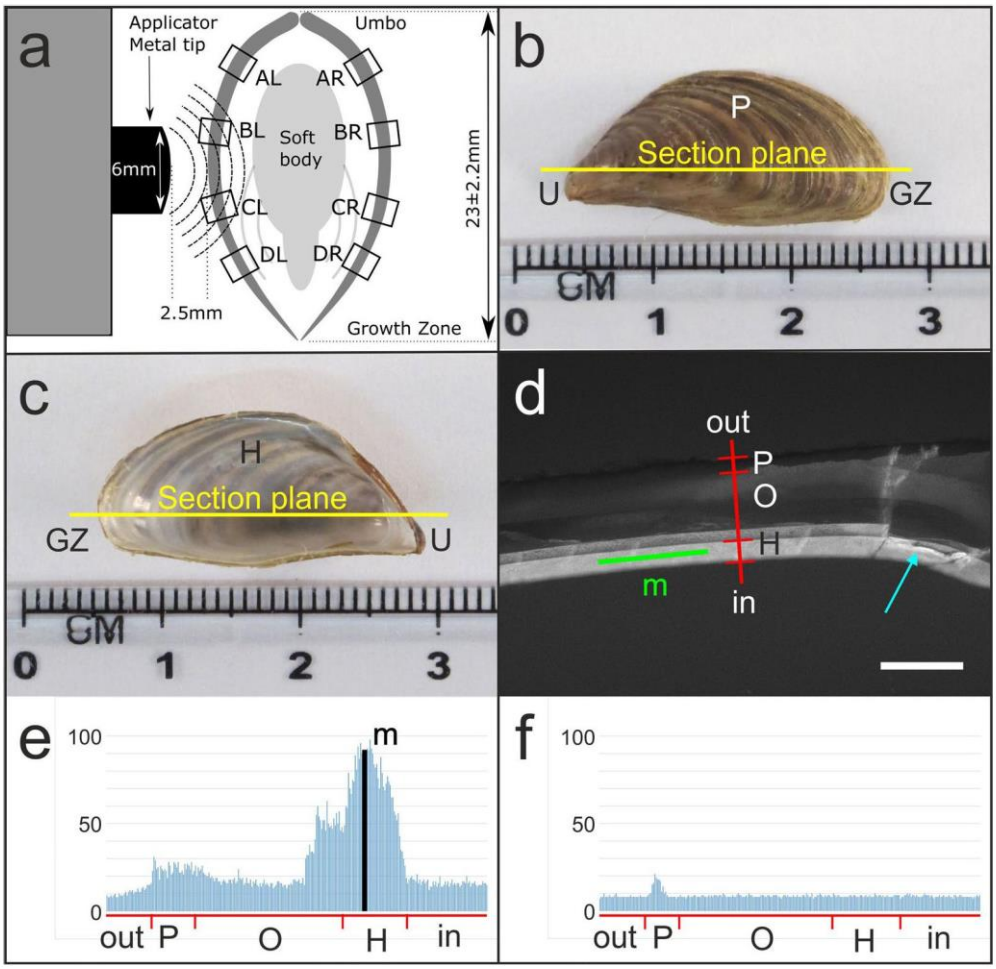

Fig. 2 Principle of exposing zebra mussels to radial extracorporeal shock waves (rESWs) and analyzing the effects on biomineralization. **a** Schematic of a cross section through a zebra mussel, indication of Regions A–D on the left (AL-DL) and the right (AR-DR) valve, and sketch of the metal applicator of the handpiece of the radial extracorporeal shock wave therapy device true to scale. **b**, **c** Side view on the valve of a zebra mussel from outside (**b**) and inside (**c**). The section plane is indicated. **d** Principle of investigating the formation of new mineralized tissue after exposure of zebra mussels to rESWs using fluorescence microscopy by determining the fluorescence signal intensity (Calcein fluorescence imaging) along the indicated green line over the hypostracum. The blue arrow indicates an artifact that was caused by the methodology used for generating the sections, resulting in irregular fluorescence signal intensity. **e**, **f** Representative linear pixel plots of the fluorescence signal intensity (in arbitrary units) along the red line shown in **d**, demonstrating high fluorescence signal intensity values specifically over the hypostracum after exposure to rESWs produced at 3.5 bar (**e**) but not after sham exposure (**f**). Abbreviations: U, umbo; P, periostracum; H, hypostracum; GZ, growth zone; out, outside surface of the muscle valve; in, inside surface of the muscle valve; m, maximum fluorescence signal intensity found over the hypostracum. The scale bar in **d** represents 300 µm

Statistical analysis

For each group of mussels (i.e., each intensity of the rESWs) mean and standard deviation of side- and region-specific fluorescence signal intensities were calculated. Outliers were identified using the Tukey's fences method [17] (with $k > 1.5$ indicating an outlier) and removed (outlier values were most probably caused by the methodology used for generating the sections, in particular by grinding and polishing). The corresponding calculations were performed using GraphPad Prism (Version 9.2.0 for Windows; GraphPad Software, San Diego, CA, USA). Fifty-seven out of the 720 individual data (six groups of mussels × 15 mussels per group × two valves per muscle × four regions per valve) (7.9%) were identified as outliers. The absolute and relative numbers of valves with 0/1/2/3/4 outlier values in their respective group were 145/21/9/2/3 and 80.6%/11.7%/5.0%/1.1%/1.7%, respectively. After removal of outliers, there were at least 12

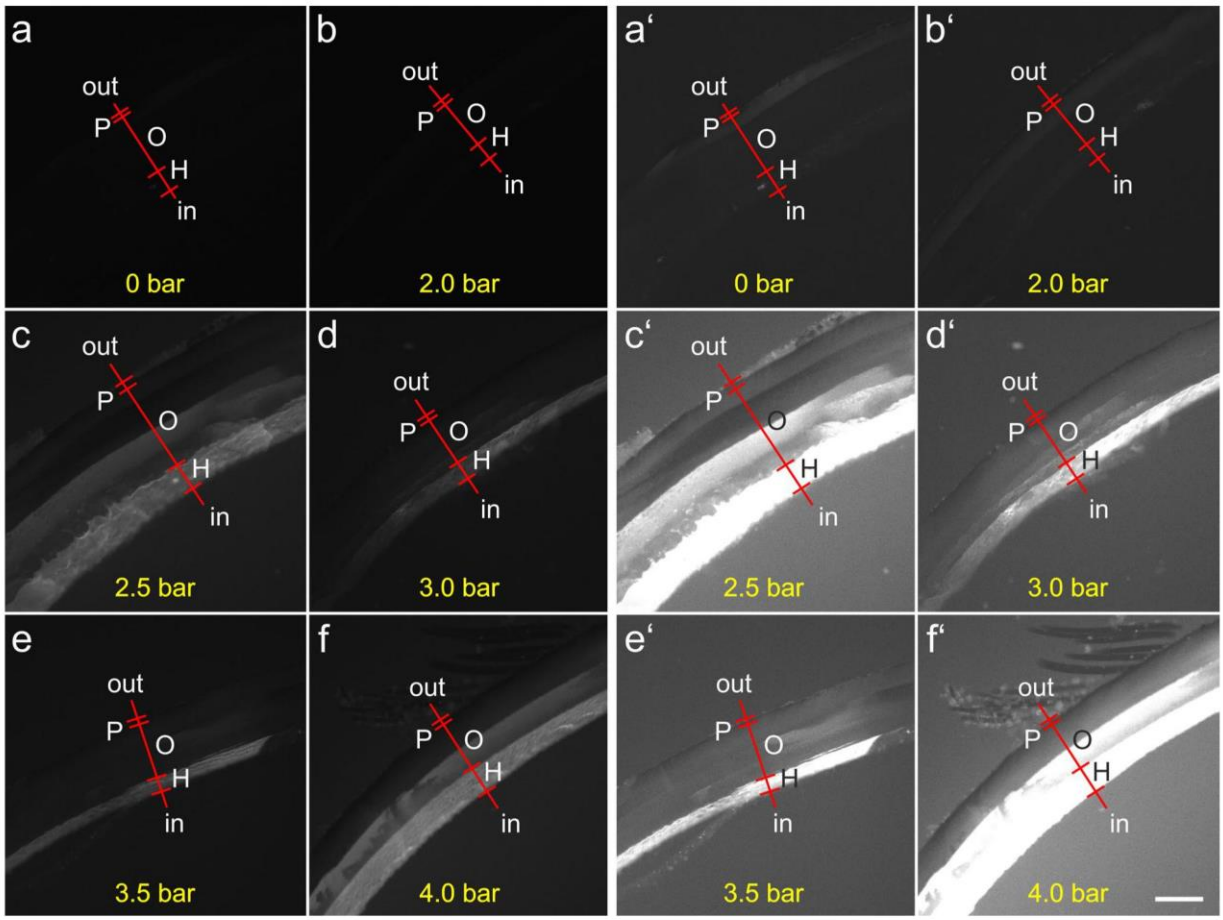

Fig. 3 Representative photomicrographs of sections of the left valve of zebra mussels exposed to radial extracorporeal shock waves as shown in Fig. 2a produced with 0 (**a**), 2.0 (**b**), 2.5 (**c**), 3.0 (**d**), 3.5 (**e**) and 4.0 (**f**) bar. In order to correctly identify the individual layers of the valves, the brightness of the images was greatly increased as shown in Panels a' to f'. Abbreviations: out, outside surface of the mussel shell; P, periostracum; O, ostracum; H, hypostracum; in, inside surface of the mussel shell. The scale bar in **f'** represents 300 µm in **a**–**f**

Table 1 Mean and standard deviation of energy-, side (left/right)- and region (regions A–D as shown in Fig. 2a)-specific fluorescence signal intensity values (arbitrary units)

Bar	AL	AR	BL	BR	CL	CR	DL	DR
0	9.9 ± 0.8 (14)	10.4 ± 1.3 (15)	10.8 ± 2.1 (15)	10.1 ± 0.8 (14)	10.7 ± 1.0 (15)	10.5 ± 0.9 (14)	9.9 ± 0.6 (15)	10.0 ± 0.7 (15)
2.0	10.8 ± 0.9 (15)	11.3 ± 2.1 (13)	10.3 ± 1.1 (15)	10.7 ± 0.9 (13)	10.6 ± 0.9 (14)	11.5 ± 1.2 (14)	10.1 ± 1.0 (14)	10.9 ± 1.3 (14)
2.5	25.7 ± 22.6 (14)	12.2 ± 3.2 (14)	12.6 ± 2.2 (12)	13.0 ± 4.3 (14)	12.4 ± 2.4 (12)	12.2 ± 2.7 (14)	15.5 ± 7.3 (15)	11.0 ± 1.4 (15)
3.0	18.9 ± 12.8 (14)	18.3 ± 12.0 (15)	17.7 ± 10.0 (14)	11.7 ± 1.7 (13)	16.7 ± 8.0 (15)	12.4 ± 2.8 (13)	10.4 ± 1.2 (13)	10.3 ± 0.7 (12)
3.5	18.3 ± 15.7 (14)	10.9 ± 3.6 (12)	13.2 ± 6.7 (13)	11.5 ± 3.3 (12)	11.1 ± 2.2 (12)	11.5 ± 3.1 (13)	10.8 ± 1.9 (13)	11.3 ± 2.9 (14)
4.0	32.8 ± 32.6 (15)	45.5 ± 51.3 (15)	30.9 ± 30.7 (14)	10.7 ± 1.3 (12)	22.4 ± 19.1 (13)	10.9 ± 0.9 (14)	12.7 ± 3.5 (14)	10.7 ± 0.9 (15)

The numbers in parentheses indicate the number of values per group after removal of outliers.

L, left; R, right

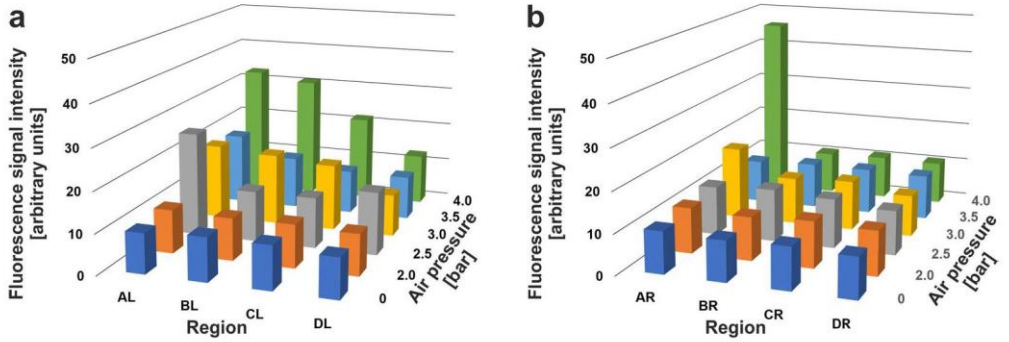

Fig. 4 3D histograms of the mean fluorescence signal intensity values found over Regions AL-DL (**a**) and AR-DR (**b**) shown in Fig. 2a as a function of the air pressure (0, 2.0, 2.5, 3.0., 3.5 and 4.0 bar) used to produce the radial extracorporeal shock waves

(out of 15 maximally possible) values available for each combination of energy, side and region.

Then, differences in mean fluorescence signal intensities were investigated using general linear model analysis, with energy (i.e., the intensity of the rESWs), side (left/exposed vs. right/unexposed) and region (regions A–D shown in Fig. 2a) as fixed factors and the averaged fluorescence signal intensities (one value each per mussel, side and region) as depending factor. Post hoc analyses (energy, region) were performed using Bonferroni's multiple comparison test. Calculations were performed using SPSS (Version 26.0.0.0; IBM, Armonk, NY, USA). *P* values smaller than 0.05 were considered statistically significant.

Results

Qualitative analysis of the left (exposed) valves indicated a dose-dependent increase in the fluorescence signal intensity particularly over the hypostracum (Fig. 3).

Table 1 summarizes mean and standard deviation of energy-, side- and region-specific fluorescence signal intensity values; Fig. 4 provides a three-dimensional (3D) graphical representation of the mean values. The results of the statistical analysis are listed in Table 2.

Figure 4 indicates energy-, side- and region-specific differences in mean fluorescence signal intensity values. In line with this, general linear model analysis demonstrated statistically significant effects of the applied shock wave energy ($p<0.001$) as well as of the side ($p=0.018$) and the investigated region ($p<0.001$) on the fluorescence signal intensity values, as well as statistically significant combined energy × region ($p<0.001$) and energy × side × region ($p=0.005$) effects (Table 2). The highest mean fluorescence signal intensity values were found in Region A, i.e., next to the umbo (Table 1). Post hoc Bonferroni tests demonstrated statistically significant differences between the mean fluorescence signal intensity values measured in Region A compared to the mean fluorescence signal intensity values measured in all other regions, but no statistically significant differences between the mean fluorescence signal intensity values measured in Regions B, C and D (Table 2). Furthermore, post hoc Bonferroni tests demonstrated statistically significant differences between the mean fluorescence signal intensity values obtained after exposure of mussels to rESWs produced at 4.0 bar and the mean fluorescence signal intensity values obtained after exposure to rESWs produced at, respectively, 0, 2.0, 2.5, 3.0 and 3.5 bar, but no statistically significant differences between mean fluorescence signal intensity values obtained after exposure to rESWs produced at respectively 0, 2.0, 2.5, 3.0 or 3.5 bar (Table 2).

Discussion

This study demonstrated that exposure of zebra mussels to rESWs had an effect on the biomineralization of the mussel valve, in a complex, dose- and region-specific manner.

The decrease in the mean fluorescence signal intensity values from the umbo (Region A) to the growth zone (Region D) found in this study was in line with earlier results obtained after exposure of zebra mussels to fESWs [10], representing the physiological mineralization process of mussel shells [18, 19]. The increased fluorescence signal intensity after exposure to rESWs was detected over the hypostracum, i.e., the shell layer which reacts with increased biomineralization after shell injuries [20, 21].

On the other hand, there was a substantial difference between the results of this study (exposure to rESWs) and our earlier study (exposure to fESWs). Specifically, after exposure of zebra mussels to fESWs, no statistically significant difference was found in the mean fluorescence signal intensity values between the exposed (left) and

Table 2 Outcome (*P* values) of the statistical analysis of the data shown in Table 1

Results of general linear model analysis										**P**
Energy										**< 0.001**
Side										**0.018**
Region										**< 0.001**
Energy × side										0.462
Energy × region										**< 0.001**
Side × region										0.509
Energy × side × region										**0.005**
Region A				**Region B**				**Region C**		
Comparison with		**P**		**Comparison with**		**P**		**Comparison with**		**P**
Results of post hoc Bonferroni tests comparing different regions (A–D, shown in Fig. 2a*) with each other*										
Region B		**< 0.001**								
Region C		**< 0.001**		Region C		1.000				
Region D		**< 0.001**		Region D		0.399		Region D		1.000
4 bar		**3.5 bar**		**3.0 bar**			**2.5 bar**		**2.0 bar**	
Comparison with	**P**	**Comparison with**	**P**	**Comparison with**	**P**		**Comparison with**	**P**	**Comparison with**	**P**
Results of post hoc Bonferroni test comparing different energy settings with each other										
3,5 bar	**< 0.001**									
3 bar	**< 0.001**	3 bar	1.000							
2,5 bar	**< 0.001**	2.5 bar	1.000	2.5 bar	1.000					
2 bar	**< 0.001**	2 bar	1.000	2 bar	0.278		2 bar	0.478		
0 bar	**< 0.001**	0 bar	1.000	0 bar	0.100		0 bar	0.185	0 bar	1.000

P < 0.05 are given boldface

unexposed (right) valves [10], which was different in this study (Fig. 4; Table 2). This was most probably caused by differences in the applied shock wave energy: exposure to fESWs was performed with EFD = 0.4 mJ/mm^2 in [10], whereas, in the present study, the highest EFD was approximately 0.11 mJ/mm^2. Thus, the lower EFD of the rESWs applied in this study was likely too low to result in a similar biological reaction (i.e., induction of biomineralization in both the exposed and unexposed valves) than the much higher EFD of the fESWs applied in our previous investigation [10]. In that study, even though the fESW energy could not reach the unexposed mussel valve, a biological reaction on both sides was triggered, probably caused by the high EFD of the fESWs applied [10]. In the present study, the energy of the rESWs was apparently high enough to activate cells of the shell epithelium to induce biomineralization in the exposed valve. However, the energy was probably too low to activate cells inside the soft body, e.g., the hemocytes carrying crystals or the crystal formation related cells [21–23]. This will be addressed in detail in future studies.

The following, unexpected results of this study could not be explained. First, the highest mean fluorescence signal intensity values were found in Region AR (i.e., on the unexposed valve) after exposure of the mussels to rESWs produced at 4.0 bar air pressure. One possible explanation was the proximity of this region to the umbo. (Note that on the exposed valve the highest mean fluorescence signal intensity values were also found in Region A.)

Second, almost no difference in the mean fluorescence signal intensity values was observed at Region AL between mussels exposed to rESWs produced at respectively 0 bar (sham exposure) or 2.0 bar air pressure, whereas the valves of mussels exposed to rESWs produced at 2.5 bar air pressure showed a much higher mean fluorescence signal intensity value at Region AL. The latter even exceeded the mean fluorescence signal intensity values at Region AL of those mussels which were exposed to rESWs produced at, respectively, 3.0 bar and 3.5 bar. The reason for this phenomenon, which occurred independently in both experiments performed in 2018 and 2019 (details not shown), is unknown. In any case, this phenomenon could indicate, for the first time, that there is no direct relationship between the applied EFD of extracorporeal shock waves (ESWs) and the extent of

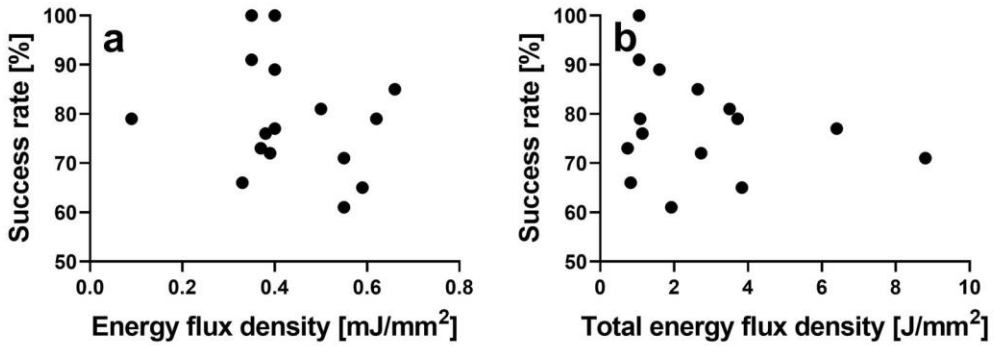

Fig. 5 Success rate (defined as the relative number of patients with radiographic union confirmed six months post focused extracorporeal shock wave therapy (fESWT)) as a function of the energy flux density (EFD) of individual focused extracorporeal shock waves (fESWs) (**a**) as well as the total EFD (individual EFD multiplied with the number of applied fESWs per treatment session and the number of treatment sessions) (**b**) in those 16 clinical studies on fESWT for treating fracture nonunions listed in Table 1 in [3] for which both the EFD of the applied fESWs and the success rate were reported

biomineralization in the target tissue. In this regard, it is of note that there was no direct relationship between the EFD of the applied fESWs and the success rate (defined as the relative number of patients with radiographic union confirmed six months post fESWT) in those 16 clinical studies on fESWT for treating fracture nonunions listed in Table 1 in [3] for which both the EFD of the applied fESWs and the success rate were reported (Fig. 5). Taken together, the results of this study may provide a reason for the phenomenon shown in Fig. 5, combined with the insight that higher EFDs beyond a certain threshold do not necessarily lead to higher success rates in treatments of fracture nonunions using ESWT. Further investigation of this phenomenon may be difficult using vertebrate animal models, considering the high number of animals which would be required. As such, exposure of zebra mussels to rESWs (as well as to fESWs) may become an attractive animal model in future research into the molecular and cellular mechanisms of ESWs in the management of fracture nonunions under consideration of the principles of the 3Rs (Replacement, Reduction, and Refinement) in research involving animal models.

Limitations

This study has several limitations. One limitation is the use of a non-vertebrate animal model in research focusing on treatments of bone injuries. However, the principles of biocalcification in invertebrates with calcified tissues, particularly mussels, show, despite their different mineral types, many similarities to those observed in vertebrate bone (details are provided in [10]). Another limitation is that this study did not contribute to better understand the molecular and cellular mechanisms of ESWs in the management of fracture nonunions. However, this was beyond the scope of this study, which focused on the analysis of the mussels' hard tissue after exposure to rESWs. A third limitation was that only one time point after exposure to rESWs was investigated. However, this may be of limited importance considering that, in the treatment of fracture nonunions with ESWT, treatment success is considered as evidence of radiographic union six months after the end of ESW treatment.

Conclusions

As in the application of fESWs, induction of biomineralization in hard tissue by exposure to rESWs may not be restricted to the region of direct energy transfer into calcified tissue. Furthermore, the results of this study may contribute to better understand why the application of higher EFDs beyond a certain threshold does not necessarily lead to higher success rates when treating fracture nonunions with ESWT.

Abbreviations

EFD: Energy flux density; ESWs: Extracorporeal shock waves; ESWT: Extracorporeal shock wave therapy; fESWs: Focused extracorporeal shock waves; fESWT: Focused extracorporeal shock wave therapy; µs: Microsecond; rESWs: Radial extracorporeal shock waves; rESWT: Radial extracorporeal shock wave therapy.

Acknowledgements

The authors thank Andrea Haderer, Claudia Harbauer and Beate Aschauer for expert technical assistance.

Authors' contributions

WW and LM carried out all experiments and performed all measurements. CS, SM and KS designed the study, analyzed and interpreted the data. WW, CS and KS drafted the manuscript. LM, JF, NM and SM reviewed and revised the manuscript. All authors approved the final version of the manuscript. All authors read and approved the final manuscript.

Funding
This study was supported by the China Scholarship Council (CSC No. 201808500132 to WW) and the Friedrich Baur foundation at LMU Munich (Reg.-Nr. 02/18 to KS).

Availability of data and materials
The datasets used and analyzed in this study are available from the corresponding author on reasonable request.

Declarations

Ethics approval and consent to participate
All experiments of this study were performed according to German animal protection regulations which do not require registration or approval of experiments using zebra mussels.

Competing interests
CS has received research funding from Electro Medical Systems (Nyon, Switzerland) (the inventor, developer and distributor of the Swiss DolorClast rESWT device) for preclinical research at LMU Munich (unrestricted grant) and consulted (until December 31, 2017) for Electro Medical Systems. However, Electro Medical Systems had no role in study design, data collection and analysis, interpretation of the data, and no role in the decision to publish and write this manuscript. No other potential conflicts of interest relevant to this article were reported.

Author details
[1]Extracorporeal Shock Wave Research Unit, Chair of Neuroanatomy, Institute of Anatomy, Faculty of Medicine, LMU Munich, 80336 Munich, Germany. [2]Department of Musculoskeletal Disorders, Faculty of Medicine and Surgery, University of Salerno, Salerno, Italy. [3]Guy Hilton Research Centre, School of Pharmacy and Bioengineering, Keele University, Stoke-on-Trent, Staffordshire ST4 7QB, England, UK. [4]Centre for Sports and Exercise Medicine, Barts and The London School of Medicine and Dentistry, Mile End Hospital, London E1 4DG, England, UK. [5]SUN Orthopedics of Evangelical Community Hospital, 210 JPM Rd, Lewisburg, PA 17837, USA.

Received: 2 November 2021 Accepted: 15 November 2021
Published online: 04 December 2021

References

1. Valchanou VD, Michailov P. High energy shock waves in the treatment of delayed and nonunion of fractures. Int Orthop. 1991;15(3):181–4. https://doi.org/10.1007/BF00192289.
2. Wang CJ, Chen HS, Chen CE, Yang KD. Treatment of nonunions of long bone fractures with shock waves. Clin Orthop Relat Res. 2001;387:95–101. https://doi.org/10.1097/00003086-200106000-00013.
3. Kertzman P, Császár NBM, Furia JP, Schmitz C. Radial extracorporeal shock wave therapy is efficient and safe in the treatment of fracture nonunions of superficial bones: a retrospective case series. J Orthop Surg Res. 2017;12(1):164. https://doi.org/10.1186/s13018-017-0667-z.
4. Schaden W, Fischer A, Sailler A. Extracorporeal shock wave therapy of nonunion or delayed osseous union. Clin Orthop Relat Res. 2001;387:90–4. https://doi.org/10.1097/00003086-200106000-00012.
5. Cacchio A, Giordano L, Colafarina O, Rompe JD, Tavernese E, Ioppolo F, Flamini S, Spacca G, Santilli V. Extracorporeal shock-wave therapy compared with surgery for hypertrophic long-bone nonunions. J Bone Joint Surg Am. 2009;91(11):2589–97. https://doi.org/10.2106/JBJS.H.00841.
6. Kertzman PF, Fucs PMB. Does radial shock wave therapy works in pseudarthrosis? Prospective analysis of forty four patients. Int Orthop. 2021;45(1):43–9. https://doi.org/10.1007/s00264-020-04778-5.
7. Gollwitzer H, Gloeck T, Roessner M, Langer R, Horn C, Gerdesmeyer L, Diehl P. Radial extracorporeal shock wave therapy (rESWT) induces new bone formation in vivo: results of an animal study in rabbits. Ultrasound Med Biol. 2013;39(1):126–33. https://doi.org/10.1016/j.ultrasmedbio.2012.08.026.
8. Schnurrer-Luke-Vrbanić T, Avancini-Dobrović V, Sosa I, Cvijanovic O, Bobinac D. Effect of radial shock wave therapy on long bone fracture repair. J Biol Regul Homeost Agents. 2018;32(4):875–9.
9. Hochstrasser T, Frank HG, Schmitz C. Dose-dependent and cell type-specific cell death and proliferation following in vitro exposure to radial extracorporeal shock waves. Sci Rep. 2016;6:30637. https://doi.org/10.1038/srep30637.
10. Sternecker K, Geist J, Beggel S, Dietz-Laursonn K, de la Fuente M, Frank HG, Furia JP, Milz S, Schmitz C. Exposure of zebra mussels to extracorporeal shock waves demonstrates formation of new mineralized tissue inside and outside the focus zone. Biol Open. 2018. https://doi.org/10.1242/bio.033258.
11. Császár NB, Angstman NB, Milz S, Sprecher CM, Kobel P, Farhat M, Furia JP, Schmitz C. Radial shock wave devices generate cavitation. PLoS ONE. 2015;10(10):e0140541. https://doi.org/10.1371/journal.pone.0140541.
12. Schmitz C, Császár NB, Milz S, Schieker M, Maffulli N, Rompe JD, Furia JP. Efficacy and safety of extracorporeal shock wave therapy for orthopedic conditions: a systematic review on studies listed in the PEDro database. Br Med Bull. 2015;116(1):115–38. https://doi.org/10.1093/bmb/ldv047.
13. Immel F, Broussard C, Catherinet B, Plasseraud L, Alcaraz G, Bundeleva I, Marin F. The shell of the invasive bivalve species dreissena polymorpha: biochemical, elemental and textural investigations. PLoS ONE. 2016;11(5):e0154264. https://doi.org/10.1371/journal.pone.0154264.
14. Claxton WT, Martel AE, Dermott RM, Boulding EG. Discrimination of field-collected juveniles of two introduced dreissenids (*Dreissena polymorpha* and *Dreissena bugensis*) using mitochondrial DNA and shell morphology. Can J Fish Aquat Sci. 1997;54(6):1280–8. https://doi.org/10.1139/cjfas-54-6-1280.
15. Data sheet FA-263/EN by Electro Medical Systems (Nyon, Switzerland).
16. Milz S, Putz R. Quantitative morphology of the subchondral plate of the tibial plateau. J Anat. 1994;185(Pt 1):103–10.
17. Tukey JW. Exploratory data analysis. Reading: Addison-Wesley Publishing Company; 1977.
18. Ramon M, Richardson CA. Age determination and shell growth of *Chamelea gallina* (Bivalvia: Veneridae) in the western Mediterranean. Mar Ecol Prog Ser. 1992;89(1):15–23. https://doi.org/10.3354/meps089015.
19. Addadi L, Joester D, Nudelman F, Weiner S. Mollusk shell formation: a source of new concepts for understanding biomineralization processes. Chem Eur. 2006;12(4):980–7. https://doi.org/10.1002/chem.200500980.
20. Beedham GE. Repair of the shell in species of Anodonta. J Zool. 1965;145(1):107–23. https://doi.org/10.1111/j.1469-7998.1965.tb02003.x.
21. Mount AS, Wheeler AP, Paradkar RP, Snider D. Hemocyte-mediated shell mineralization in the eastern oyster. Science. 2004;304(5668):297–300. https://doi.org/10.1126/science.1090506.
22. Li S, Liu Y, Liu C, Huang J, Zheng G, Xie L, Zhang R. Hemocytes participate in calcium carbonate crystal formation, transportation and shell regeneration in the pearl oyster *Pinctada fucata*. Fish Shellfish Immunol. 2016;51:263–70. https://doi.org/10.1016/j.fsi.2016.02.027.
23. Song X, Liu Z, Wang L, Song L. Recent advances of shell matrix proteins and cellular orchestration in marine molluscan shell biomineralization. Front Mar Sci. 2019;6:41. https://doi.org/10.3389/fmars.2019.00041.

Publisher's Note

3.2 Paper II

Article

Immunohistochemical Detection of Various Proteoglycans in the Extracellular Matrix of Zebra Mussels

Wenkai Wu [1], Juergen Geist [2], Sebastian Beggel [2], Christoph Schmitz [1], Stefan Milz [1,*] and Katharina Sternecker [1]

[1] Institute of Anatomy, Faculty of Medicine, LMU Munich, D-80336 Munich, Germany; wenkai.wu@med.uni-muenchen.de (W.W.); christoph_schmitz@med.uni-muenchen.de (C.S.); katharina.sternecker@med.uni-muenchen.de (K.S.)
[2] Aquatic Systems Biology Unit, TUM School of Life Sciences, Technical University of Munich, D-85354 Freising, Germany; geist@tum.de (J.G.); sebastian.beggel@tum.de (S.B.)
* Correspondence: stefan.milz@med.uni-muenchen.de; Tel.: +49-89-2180-72633

Abstract: Mussels have been used as animal models for studying ecotoxicology, biomineralization, and bio-adhesion for many years. Despite a wealth of studies on their shell matrix and byssus proteins, few studies have focused on the extracellular matrix molecules in mussel soft tissues. Extracellular matrix molecules may play important roles in biomineralization, immune reaction, and tissue homeostasis. In the present study, extracellular matrix and mineralization-related molecules in zebra mussel soft tissue were immunolocalized using well-characterized monoclonal antibodies. Our results demonstrate specific immunolocalization for collagen IV, fibronectin, and keratan sulfate in hemocytes; collagen IV in peripheral nerves; and aggrecan, link protein, and collagen XVIII in foot tissue. Laminin, decorin, and osteonectin were also broadly immunolocalized in mussel soft tissues. The distributions of these extracellular matrix molecules in mussel tissues are in line with the cell-mediated shell mineralization hypothesis, providing evidence for the molecules involved in the peripheral nervous system and byssus formation, and explaining the conservation of extracellular matrix molecules during evolution. These results further contribute to establishing zebra mussels as an attractive animal model in biomedical research.

Keywords: zebra mussel; extracellular matrix; biomineralization; mollusk; proteoglycans; adhesion

Citation: Wu, W.; Geist, J.; Beggel, S.; Schmitz, C.; Milz, S.; Sternecker, K. Immunohistochemical Detection of Various Proteoglycans in the Extracellular Matrix of Zebra Mussels. *Fishes* **2022**, *7*, 74. https://doi.org/10.3390/fishes7020074

Academic Editor: Maria Angeles Esteban

Received: 1 February 2022
Accepted: 22 March 2022
Published: 24 March 2022

1. Introduction

Mollusks are the second-largest phylum of invertebrate animals on earth, occurring in marine, freshwater, and terrestrial habitats [1]. They comprise a diversity of marine and freshwater mussels and clams (also referred to as bivalves) which play an important role in ecosystem processes, e.g., by contributing to water purification [2–4] or acting as ecological engineers [5]. In addition, mussels have also become prominent targets of bionics and human-centered research. Biomineralization mechanisms of shells, bio-adhesive molecules in byssus, and bio-indicator usages for the detection of toxic chemicals [6,7] have all been of particular interest. However, apart from the shell and byssus, few studies have dealt with the extracellular matrix of the soft body tissues within bivalves [8].

The extracellular matrix is a cell-secreted and -maintained three-dimensional framework present in almost all tissues and organs. The emergence of the extracellular matrix promoted the evolution from unicellular organisms to multicellular organisms. The extracellular framework plays important roles in tissue organization, modulation of innate immune response, cell adhesion, and structural support [9], as well as in signal transduction and regulation of many cell functions during growth, differentiation, migration, regeneration, and degeneration [10]. The extracellular matrix contains collagen, proteoglycans, glycosaminoglycans, many glycoproteins, and, in certain cases, enzymes [11]. During the evolution of Metazoa from the sponges to vertebrates (including the human species), a

surprisingly large number of extracellular matrix components were conserved [12]. The investigation of extracellular matrix molecules in different species can help to better understand the evolutionary path of biological structures, functions, mechanisms in certain tissues, and the effects of pathogens or toxicants on these functions and mechanisms. This especially relates to mineralized tissues, because, despite the universal use of calcium as a prevailing mineral, mussels and vertebrates differ regarding the use of certain anions [13].

The present study was conducted using soft tissues of the zebra mussel (*Dreissena polymorpha*) which is a well-explored animal model in environmental and toxicological studies [14,15]. Zebra mussels can be bred and maintained under controlled laboratory conditions, which allows systematic testing of external factors on this species. In an environmental context, they are already used as bioindicators, for example, to assess chemical contamination since they are sessile animals and represent the conditions from the site they were collected [16].

Shell mineralization in mussels has been regarded as a prototypical biomineralization model in nature. Consequently, we previously used zebra mussels for studying the stimulation of bio-mineralization after exposure to extracorporeal shock waves [17,18]. The motivation behind these studies was the fact that extracorporeal shock wave therapy (ESWT) is one of the most promising approaches for treating fracture nonunions [19]; however, the underlying molecular and cellular mechanisms of induced bio-mineralization following ESWT are only poorly understood and cannot be comprehensively investigated in a realistic context using cell culture models only. We also used zebra mussels for studying disturbed bio-mineralization after exposure to possible aetiological factors of molar–incisor hypomineralization (MIH) (including bisphenol-A), which may pave the way for better understanding of the pathogenesis of MIH, for which no treatment is currently available [20].

In comparison with human osteoblast- and osteoclast-mediated mineralization [21,22], the question arises whether the mineralization-related extracellular matrix molecules typically present in mammalian mineralized tissues are also present in certain mussel soft tissues. To address this question, a panel of well-characterized monoclonal antibodies that have previously been demonstrated in mammalian (especially human) extracellular matrix tissues were selected for immunohistochemical staining. The set of antigens investigated in this study comprises collagens, glycosaminoglycans, proteoglycans, and basal lamina-related antigens. Specifically, we hypothesized a high degree of conservation of certain extracellular matrix molecules during evolution. Therefore, we demonstrate that a set of antibodies, originally developed for use in mammalian tissues, are also recognizing epitopes in zebra mussel soft tissue.

2. Materials and Methods

All mussels (n = 7, 3 males and 4 females) investigated in this study originated from the river Ischler Achen (Upper Danube Drainage, Bavaria, Germany) and from the river Schinderbach (Bavaria, Germany) in July 2014 and February 2020. Mussels with a shell length of over 2 cm from anterior to posterior were selected and maintained in individual holding units at the Aquatic System Biology Unit, Technical University of Munich (Freising, Germany). The mussels were incubated in multi-well plates (VWR catalog number: 734–2323, VWR part of Avantor, Radnor, Pennsylvania, U.S.) which were fixed in a bucket. The bucket was filled with 10 L groundwater (dissolved oxygen 12.5 ± 2.1 mg/L, pH 7.98 ± 0.21, electric conductivity at 20 °C 1049 ± 55 mS/cm^2) at a mean temperature of 12.5 °C and with 30% of the water changed daily. Mussels were fed by adding 0.2 mL/L Shellfish Diet 1800 (Reed Mariculture, Campbell, CA, USA) to the incubation water once per week before the immunohistochemical experiments were conducted [23,24].

All experiments were performed according to German animal protection regulations. No requirement of registration or approval of experiments was necessary for the investigation of zebra mussels, which are considered invasive invertebrates in Germany.

Mussels were acclimatized to experimental conditions for 2 weeks before sacrificing them by immersion into 70% (v/v) ethanol for 48 h. Shells were opened by severance of

the adductor muscle. Soft bodies were carefully removed and post-fixed in 70% ethanol followed by standard gradient dehydration and subsequent embedding in paraffin (short protocol: 70%, 80%, 96%, 100%, 100% ethanol (dehydration), xylol-1, xylol-2 (clearing), paraffin-1, paraffin-2, paraffin-3 (embedding), 3 h for all steps mentioned). Alcohol fixation has proven useful in studying mammalian tissues, preserving the antigenicity of the extracellular matrix antigens that we aimed to investigate in this study. Routine paraffin embedding was processed using an automated tissue processor (Leica ASP 200S; Leica Microsystems, Nussloch, Germany). Using a LEICA SM2010R microtome (Leica Biosystems), paraffin blocks were serially sectioned into slides of 7 µm thickness along the standard ventral–dorsal plane, allowing all major organs and tissues (mantle, gill, digestive gland, gonad, foot, and byssus gland) to be incorporated into one single histological section [25]. A sketch drawing of mussel soft body sections in the cutting plane is shown in Figure 1 with anatomical structures marked [26]. For immunohistochemical labeling, a distinct magenta chromogen (EnVision FLEX HRP Magenta Substrate Chromogen System, GV925; Dako, Copenhagen, Denmark) was chosen because the mussels contained high quantities of dark brown endogenous pigment and the reddish color of the magenta chromogen was better discernable from it.

Sections were processed with immunohistochemistry using a panel of mouse monoclonal antibodies against collagens (type IV and XVIII), glycosaminoglycans (chondroitin 4 and 6 sulfates and keratan sulfates), proteoglycans (aggrecan, link protein, versican, decorin), and other matrix proteins (fibronectin, laminin, osteonectin). Reduction and alkylation were conducted according to a scheme described in Milz et al. [27] and were applied prior to the enzyme pretreatment. The activity of endogenous peroxidase was blocked with 3% (*v/v*) hydrogen peroxide in methanol for 30 min and the non-specific binding was reduced by incubating sections with 2.5% (*v/v*) normal horse serum (S-2012, Vector Laboratories, Burlingame, CA, USA) for 60 min at room temperature. Antibody binding was detected with a sensitive Dako EnVision+ System- HRP Labeled Polymer (K4001; Dako, Copenhagen, Denmark) and visualized with an EnVision FLEX HRP Magenta Substrate Chromogen System (GV925; Dako, Copenhagen, Denmark), resulting in a strong, reddish signal. Counterstaining was performed using Mayer's hematoxylin. For control sections, the primary antibody was replaced by phosphate-buffered saline. Primary antibody incubation was performed overnight at 4 degrees Celsius in a moist chamber. The secondary antibody detection system (Dako EnVision+ System-HRP Labeled Polymer, K4001; Dako, Copenhagen, Denmark) was used according to the manufacturers' recommendation. An example protocol of the entire procedure is provided in Table 1; full details of the antibodies and specific pretreatments are provided in Table 2.

A potential obstacle relates to the fact that mussel hemocytes contain several enzymes [28], and the peroxidases, especially, might react with the magenta chromogen visualization system, which could result in false positives. In order to avoid this, the endogenous peroxidases were inactivated with 3% hydrogen peroxide in methanol for 30 min. Compared to other immunohistochemical protocols, usually applied in mammalian tissues, this is a long blocking step which we adopted after several pilot trials conducted for optimization of the labelling procedure. A further methodological precaution was to strictly limit the time for the magenta chromogen incubation to 5 min to avoid non-specific background staining.

The specimens were analyzed with a light microscope (Axiophot Photomicroscope, Carl Zeiss Microscopy, Oberkochen, Germany) equipped with Plan-Neofluar objectives (20×/0.50, 40×/0.75 Carl Zeiss Microscopy, Oberkochen, Germany) and an Axiocam HRc (Carl Zeiss Microimaging, Goettingen, Germany) digital camera using Zeiss Axiovision software (version 4.9.1 SP2). Photographs were taken at the same magnification and exported as TIFF files, which were finally adjusted for brightness and contrast using Adobe Photoshop CS4 (version 11.0; Adobe Systems, CA, USA). Care was taken that the original appearance of the material remained unchanged.

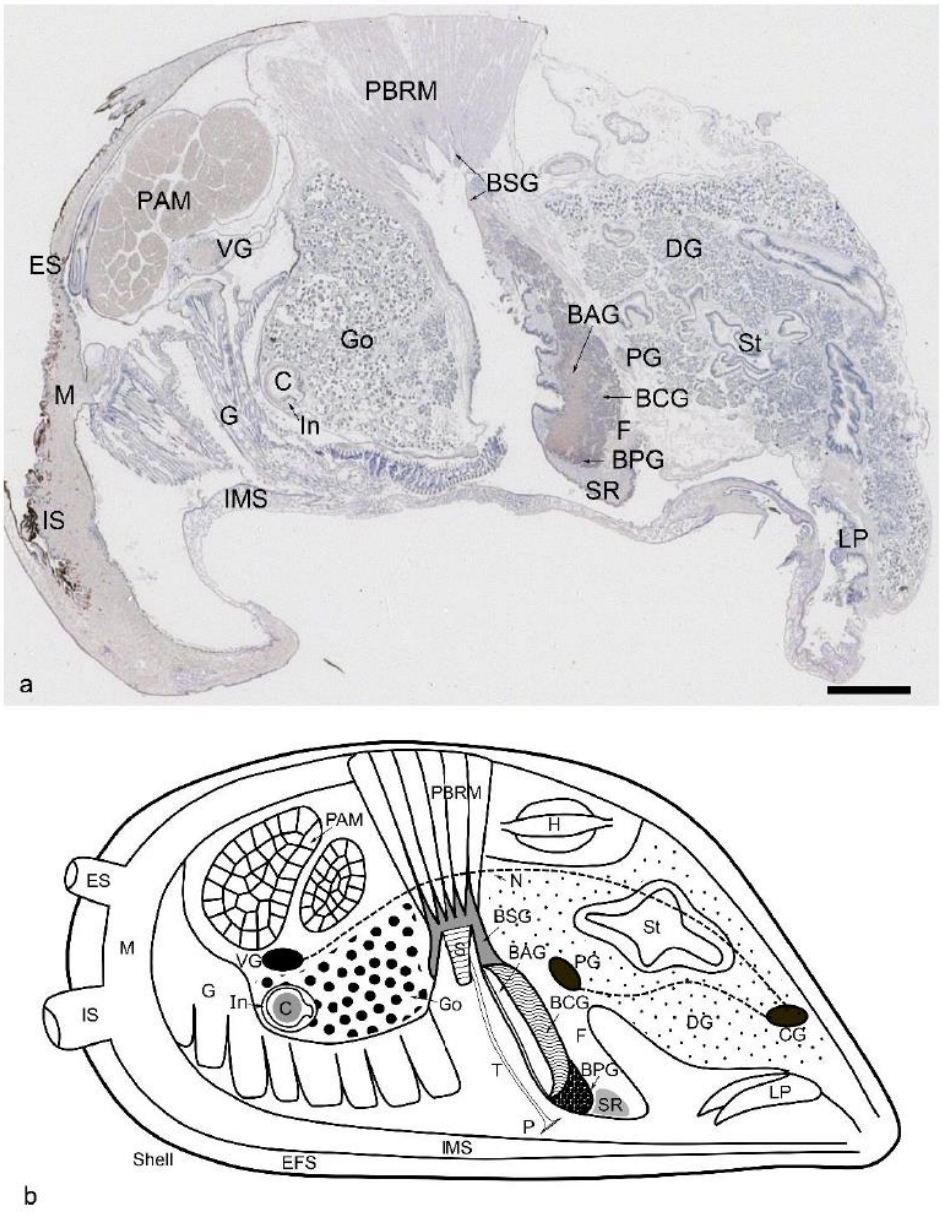

Figure 1. Overview of a *Dreissena polymorpha* mussel soft body histology section stained with Mayer's hematoxylin (**a**) and a sketch drawing of the soft body with the most important anatomical structures indicated (**b**). The scale bar in (**a**) represents 1 mm. Note that not all structures shown in the sketch drawing are visible in the histological section. The mussel's body is surrounded by mineralized tissues (shells) which are represented by the outer thick black line. The soft tissue next to the shell is the mantle (M), which is involved in the cell-mediated mineralization process. The two shell valves are connected by the muscles (PAM, posterior adductor muscle), foot (F), and byssus apparatus (containing the byssal stem (S), byssus thread (T), byssus plaque (P), byssus stem gland (BSG), byssus accessory gland (BAG), byssus collagen gland (BCG), byssus phenol gland (BPG), and posterior byssal retractor muscle (PBRM)). The muscles are innervated by nerves and ganglia (PG: pedal ganglion, VG: visceral ganglion, CG: cerebral ganglion, N: peripheral nerves). The intestinal system has several parts (DG: digestive glands, St: stomach, C: crystalline style, LP: labial palp) and is in close connection to the gills (G) and gonads (Go). Additional abbreviations: IMR, inter mantle region; IS, inhalant siphon; ES, exhalant siphon; EFS, extrapallial fluid space; SR, the subepithelial region in the distal foot.

Table 1. Immunohistochemistry protocol for detection with the DAKO Envision system. All steps were performed at room temperature if not otherwise stated.

Step	Procdure	Time/Temperature
1	Removal of paraffin with Xylene	3 × 5 min
2	Descending Alcohols	
2a	100% Ethanol	2 × 5 min
2b	90% Ethanol	1 × 5 min
2c	80% Ethanol	1 × 5 min
2d	70% Ethanol	1 × 5 min
2e	Tap water	1 × 5 min
3	Reduction and Alkylation protocol to be performed here, if necessary	
3a	To prepare reduction buffer (250 mL), (i) dissolve 50 mM Tris (121,1 g/mol; 1.51 g) and 200 mM NaCl (58.4 g/mol; 2.92 g) in 200 mL distilled H_2O; (ii) measure pH and bring to 7.35 pH with HCl; then (iii) add distilled H_2O until 250 mL *	
3b	Reduction working solution: DTT 10 mM (100 mL reduction buffer + 0.154 g DTT)	2 h at 37 °C
3c	Alkylating working solution: iodoacetamide 40 mM (0.74 g in 100 mL PBS) **	1 h at 37 °C
4	Washing with PBS + Tween	1 × 5 min
5	3% Hydrogen peroxide in methanol (10 mL 30% H_2O_2 + 90 mL 100% methanol)	30 min
6	Washing with PBS + Tween	3 × 5 min
7	Enzyme pre-treatment (primary antibody specific)	30 min at 37 °C
8	Washing with PBS + Tween	3 × 5 min
9	Blocking with 2.5% normal horse serum (vector RTU) (discard excess serum; do not wash)	60 min
10	Primary antibody incubation in moist chamber (control with PBS)	Overnight at 4 °C
11	Washing with PBS + Tween	3 × 5 min
12	DAKO EnVision System (K4001) for mouse primary antibodies (goat anti-mouse secondary antibody labelled with HRP-polymer) in moist chamber	30 min
13	Washing with PBS + Tween	3 × 5 min
14	Dako EnVision Flex magenta chromogen (GV925)	5 min
15	Washing with tap water	1 × 5 min
16	Counterstaining with Mayer's hematoxylin	20 s
17	De-staining with tap water	15 min
18	Mounting and coverslipping with Kaiser's Glycerol Gelatine	

Notes: * This solution can be stored for approximately one week in a fridge at 4 °C. ** Iodoacetamide stabilizes broken disulphide bonds and thus retains the reduction state for a longer period, despite the air oxygen, which reverses the reduction by oxidation; therefore, sections can be kept in a moist chamber and stored in a fridge at 4 °C overnight. The immunohistochemical protocol can be performed on the following day. Abbreviations: DTT, 1,4-dithiothreitol (Cleland's reagent); h, hour; HRP, horse radish peroxidase; min, minutes; mM, millimolar; PBS, phosphate-buffered saline; sec, seconds; RTU, ready-to-use; Tris, Tris base (2-amino-2-(hydroxymethyl)-1,3-propanediol); Tween, Tween 20 (polyethylene glycol sorbitan monolaurate) (use at 0.1%).

Table 2. List of monoclonal antibodies used in this study, together with their dilutions, pretreatments, and sources. All the antibodies are mouse monoclonals. Abbreviations: DSHB, developmental studies hybridoma bank; Ch ACII, chondroitinase ACII (Sigma); Ch ABC, chondroitinase ABC (Sigma); Hyal, hyaluronidase (Sigma). Antibodies 2B6, 3B3,1/20/5-D-4 were gifts from B. Caterson.

Antigen	Antibody	Dilution	Pretreatment	Source
Collagen IV	M3F7	1:5	Hyal. (1.5 U mL^{-1})	DSHB
Collagen XVIII	6C4	1:5	PBS	DSHB

Table 2. *Cont.*

Antigen	Antibody	Dilution	Pretreatment	Source
Chondroitin-4 sulfate	2B6	1:150	Ch. ACII (0.125 U mL^{-1})	B. Caterson
Dermatan and chondroitin-4 sulfate	2B6	1:150	Ch. ABC (0.25 U mL^{-1})	B. Caterson
Chondroitin-6 sulfate	3B3	1:80	Ch. ABC (0.25 U mL^{-1})	B. Caterson
Keratan sulfate	1/20/5-D-4	1:150	PBS	B. Caterson
Keratan sulfate	MZ15	1:5	PBS	DSHB
Decorin/dermatan sulfate proteoglycan	DS1	1:5	Ch. ACII (0.125 U mL^{-1})	DSHB
Decorin/dermatan sulfate proteoglycan	CB-1	1:5	Ch. ACII (0.125 U mL^{-1})	DSHB
Fribronectin	HFN 7.1	1:5	PBS	DSHB
Aggrecan	12/21/1-C-6	1:5	Reduction & Alkylation Ch. ACII (0.125 U mL^{-1})	DSHB
Link protein	9/30/8-A-4	1:5	Reduction & Alkylation Ch. ACII (0.125 U mL^{-1})	DSHB
Osteonectin	AON1	1:5	PBS	DSHB
Laminin	2E8	1:5	PBS	DSHB

3. Results

All mussel individuals presented consistent staining patterns in somatic and gonad tissues. The results of immunohistochemical labeling could be broadly categorized as follows: (i) Antibodies for collagen IV (M3F7), collagen XVIII (6C4), fibronectin (HFN7.1), keratan sulfate (MZ15), chondroitin-4 sulfate, and dermatan sulfate (2B6, with chondroitinase ABC/AC pretreatment), aggrecan (12/21/1-C-6), and link protein (9/30/8-A-4) labeled distinct anatomical structures in zebra mussel soft tissues. The results for all antibodies which labeled at least one region of the zebra mussel soft tissue are summarized in Table 3. (ii) Antibodies for laminin (2E8), decorin (CB-1, DS1), and osteonectin (AON-1) labeled many structures in zebra mussel soft tissues, without preference for a particular cell or tissue type. (iii) Positive labeling of keratan sulfate antibody MZ15 in hemocytes was not matched by another keratan sulfate antibody (1/20/5-D-4), which did not result in any labeling in zebra mussel soft tissues. (iv) Antibodies for chondroitin-6 sulfate (3B3, with chondroitinase ABC pretreatment) did not label any zebra mussel soft tissue. The immunohistochemical results of this study were not influenced by the sex of the mussels, except a higher number of hemocytes in testis than ovaries are cited.

3.1. Collagen IV, Fibronectin, and Keratan Sulfate (MZ15)

Collagen IV antibody was strongly labeled in the peripheral nerves and parts of the ganglions (including the visceral, pedal, and cerebral ganglions) of zebra mussels (Figure 2a–d). Within the intensively stained nerves, individual cell nuclei (of glia or supporting cells) could be recognized along with each axon (inset in Figure 2c). The labeled regions of ganglions were located mainly in the transition zone from the ganglion to the peripheral nerves and did not cover perikarya (Figure 2c). Along with the nerve and ganglion, some positively labeled hemocytes could be observed as well (Figure 2c). Besides collagen IV, fibronectin and keratan sulfate (MZ15) antibodies were both strongly positive in hemocytes, with distribution in the gonads, gills, muscle tissues, and central and edge regions of the mantle. Distribution of the positive hemocytes was mainly in the gonads (among germinal tissue of testis (Figure 2e,f) and side regions of ovaries), gills, inter-mantle spaces (central mantle region, shown in Figure 2i), mantle edge regions (Figure 2g,h), and among muscle fibers (Figure 2j,k). Although most hemocytes were labeled by the three antibodies, a small number of hemocytes remained unlabeled.

The positive hemocytes were mainly large, round, hyalinocytes-like cells, with strong positive reactions in the cytoplasm (Figure 2e,i). No significant morphological difference was noticed within those positive hemocytes. A large number of immunopositive hyalinocyte-like cells could be observed in the gonads (Figure 2e,f), as described by Evariste et al. [29].

Table 3. Summary of the immunohistochemical labeling profile of specific regions of the soft body of *Dreissena polymorpha* found in this study. Results for antibody labeling per region. The numbers indicate the number of positive labeled regions ($n = 7$ specimens per group, 3 males and 4 females). (Abbreviations: Go: gonads, G: gill, M: mantle, IMS: inter-mantle space, PG: pedal ganglion, VG: visceral ganglion, CG: cerebral ganglion, PAM, posterior adductor muscle, PBRM: posterior byssal retractor muscle, BSG: byssus stem gland, BCG: byssus collagen gland, BAG: byssus accessory gland, SR: subepithelial region in the distal foot, St/In: stomach/intestine lamina propria, C: crystalline style, DSP: dermatan sulfate proteoglycan, C6s: chondroitin-6 sulfate, C4s: chondroitin-4 sulfate.)

	Hemocytes				**Nervous System**		**Muscle**	**Foot**				**Digestive Organs**	
Antigen	Go	G	M	IMS	PG/VG/CG	N	PAM/PBRM	BSG	BCG	BAG	SR	St/In	C
Collagen IV	7	7	7	7	4	7	0	0	0	0	0	0	0
Collagen XVIII	0	0	0	0	0	0	7	0	0	0	5	0	0
Fribronectin	4	4	2	4	0	0	3	0	0	0	0	0	0
Keratan sulfate (MZ15)	7	7	6	7	0	0	0	0	0	0	0	0	0
C4s (2B6 + Ch.ACII)	0	0	0	0	0	0	0	0	0	0	0	7	4
Dermatan and C4s (2B6 + Ch.ABC)	0	0	0	0	0	0	0	0	0	0	0	7	4
Aggrecan	0	0	0	0	0	0	7	7	4	5	0	2	0
Link protein	0	0	0	0	0	0	7	7	0	0	0	5	0
Osteonectin	5	5	5	5	4	4	5	4	4	3	4	4	0
Laminin	6	6	6	6	4	5	7	7	4	3	4	5	0
Decorin/DSP (DS1)	7	7	7	7	4	7	7	7	3	3	5	5	0
Decorin/DSP (CB-1)	7	7	7	7	4	7	7	7	3	3	5	5	0
C6s (3B3 + Ch.ABC)	0	0	0	0	0	0	0	0	0	0	0	0	0
Keratan sulfate (1/20/5-D-4)	0	0	0	0	0	0	0	0	0	0	0	0	0

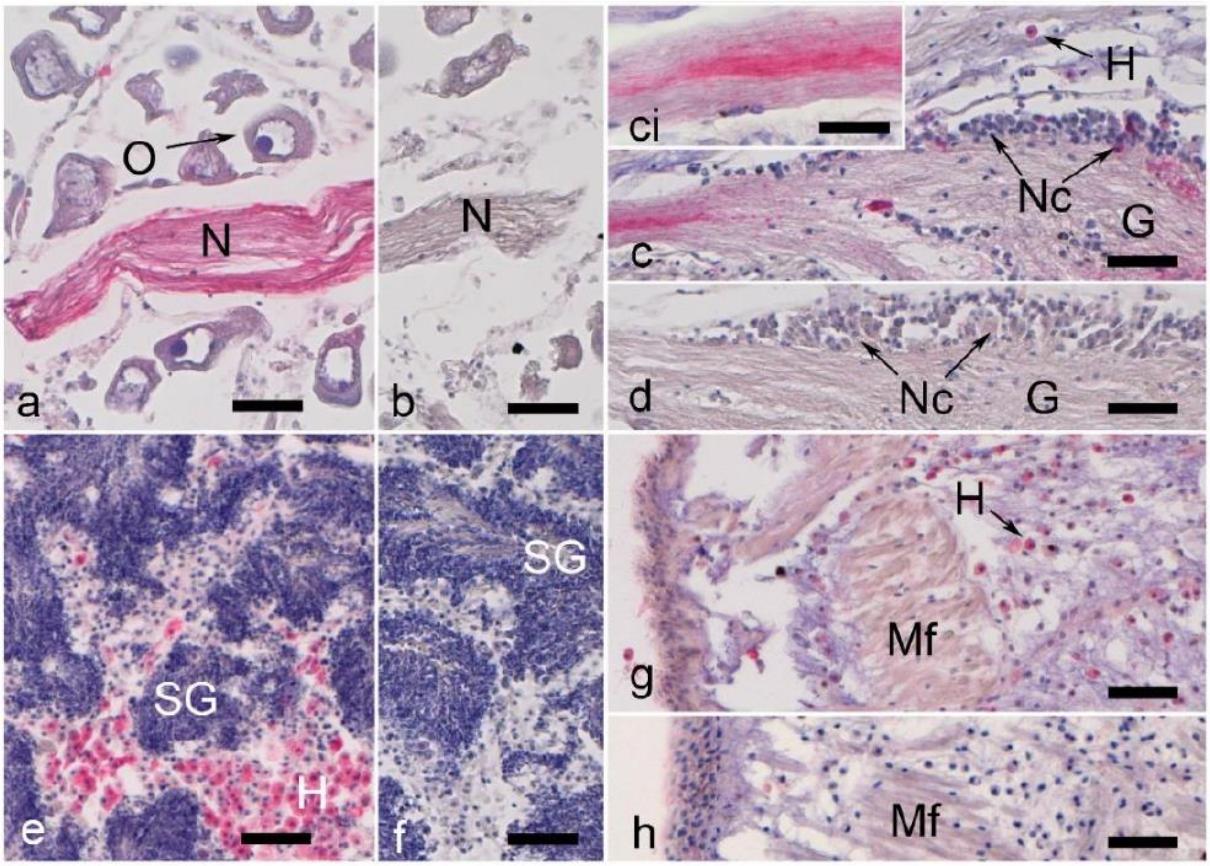

Figure 2. *Cont.*

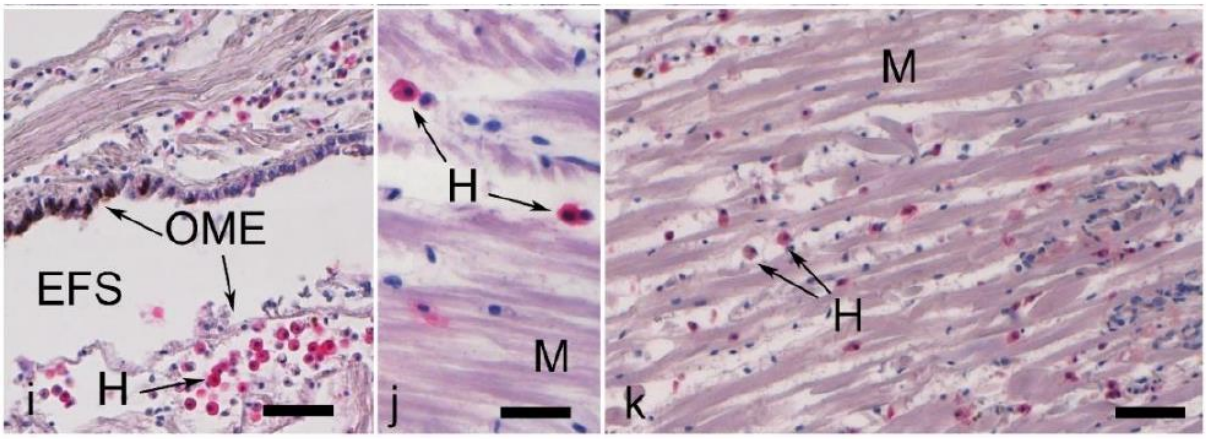

Figure 2. Nerve and hemocyte labeling in *Dreissena polymorpha* tissue (the immunohistochemical signal is in magenta). All scale bars represent 50 µm, with the exception of the inset (*) in (**c**,**j**), which is 25 µm. (**a**) Collagen IV-labeled nerve fiber bundle surrounded by non-labeled oocytes (O). (**b**) Control to (**a**), showing a nerve fiber bundle (N). (**c**) Partially collagen IV-labeled ganglion (G). Note that most of the nerve cells (Nc) are not labeled, while the branching fibers show dye deposits. This is shown at higher magnification in the inset in (**c**). (**d**) Control to (**c**). (**e**) Collagen IV-positive hemocytes (H) in the germinal tissue of testis (T). Note that the tissue used for spermiogenesis (SG) is not labeled. (**f**) Control to (**e**). (**g**) Fibronectin labeling of hemocytes (H) in mantle edge region; muscular fibers (Mf) remain unstained. (**h**) Control to (**g**). (**i**) Distinct labeling for collagen IV exhibited by a number of hemocytes (H) in the central mantle. Note that not all hemocytes are labeled. Furthermore, the outer mantle epithelium (OME) in the mantle edge region exhibits a dark brown pigmentation. EFS: extrapallial fluid space. (**j**) Muscle tissue with collagen 4-positive labeled hemocytes. The muscle fibers are not labeled. (**k**) Keratan sulfate (antibody MZ15) labeling in a few hemocytes among muscle fibers (M).

3.2. Aggrecan, Link Protein, Collagen XVIII, and Glycosaminoglycans

Immunolabeling for aggrecan and link protein was found in muscle fibers (Figure 3a–c), byssus stem gland cells (Figure 3a–c), and the lamina propria of the stomach and intestine (Figure 3e,f). Aggrecan immunolabeling was also found in the accessory and collagen glands (Figure 3d) in the foot. In the distal part of the foot, a specific subepithelial region was found to react positively with the collagen XVIII antibody (Figure 3g,h). This region was located at the ventral side of the distal foot, which was next to the plaque-forming gland.

Moreover, the anti-chondroitin sulfate antibody 2B6 was used to identify and locate neoepitopes of chondroitin-4-sulfate (pre-digested with chondroitinase ABC) and dermatan sulfate GAG chains (pre-digested with chondroitinase ACII). Both pre-treatment methods showed immunopositive signals with particular concentrations in the crystalline style (Figure 3i,j) and the lamina propria of the stomach and intestine.

3.3. Laminin, Osteonectin, and Decorin

Laminin, osteonectin, and two types of decorin (DS1 and CB-1)-recognizing antibodies were broadly positive in almost all studied mussel soft tissues (mantle, muscular fibers, connective tissue (Figure 3k–m), nervous system, gill, digestive gland, gonads, and foot).

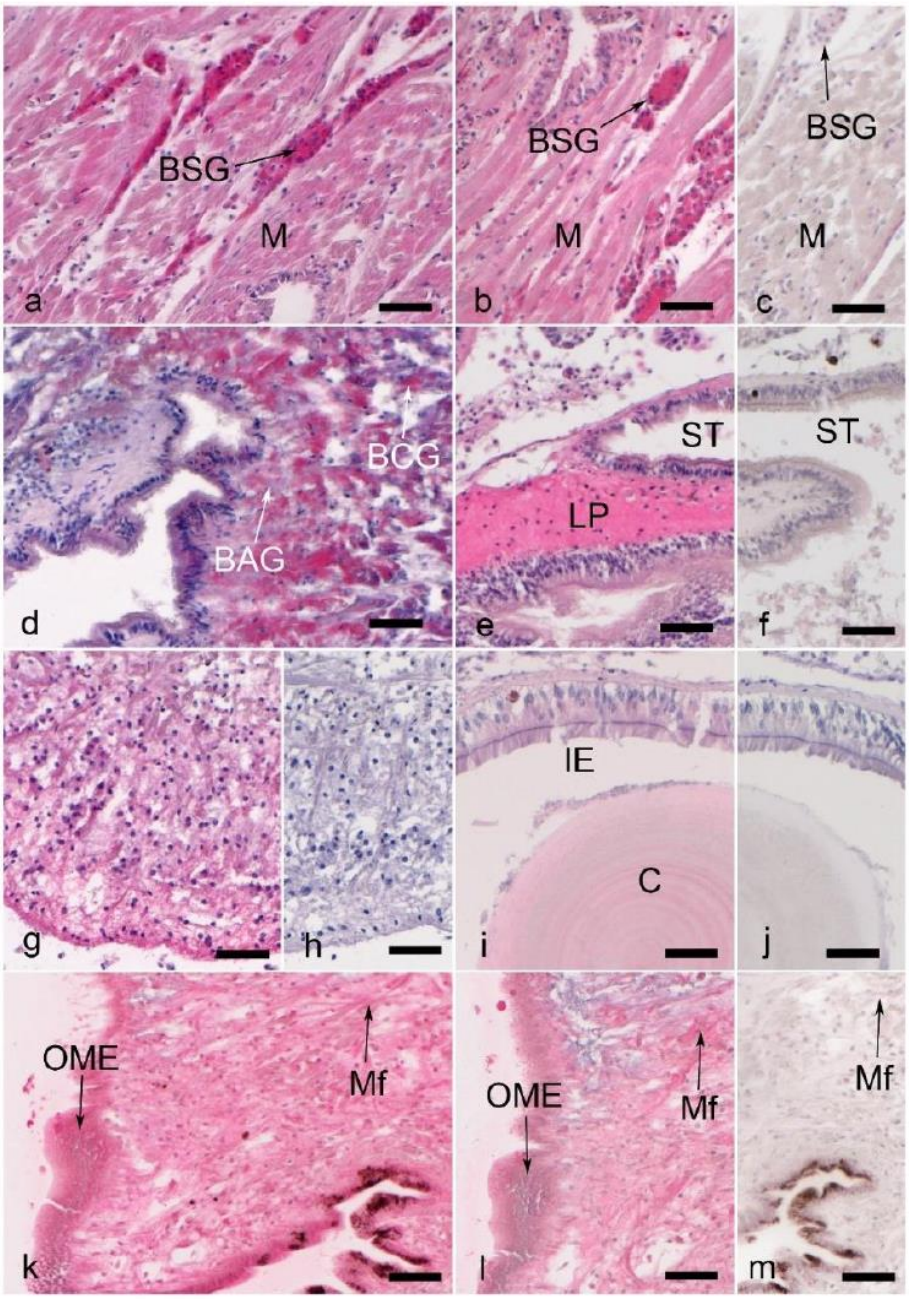

Figure 3. Muscle, foot, byssus gland, and intestinal labeling with proteoglycans and glycosaminoglycans in *Dreissena polymorpha* tissue (immunohistochemical signal is in magenta). All scale bars represent 50 µm. (**a**) Strong labeling for aggrecan and (**b**) link protein in byssus stem gland (BSG) cells within posterior byssal retractor muscles (M). (**c**) Muscle (M) and byssus stem gland (BSG) tissue, control to (**a**,**b**). (**d**) Aggrecan labeling in byssus collagen (BCG) and accessory gland (BAG) cells. (**e**) Link protein labeling in stomach (ST) lamina propria tissue (LP). (**f**) Control to (**e**). (**g**) Collagen XVIII labeling in the subepithelial region of the distal foot (SR in Figure 1). (**h**) Control to (**g**). (**i**) Chondroitin-4 sulfate labeling in the crystalline style (C) and some intestinal epithelial cells (IE). (**j**) Control to (**i**). (**k**) Mantle edge tissue labeled with an antibody against decorin (DS1), while (**l**) shows the decorin labeling with decorin antibody CB-1 in the same tissue. (**m**) Control to (**k**,**l**). Mf: muscular fibers; OME: outer mantle epithelium.

4. Discussion

As a notorious invasive species, the zebra mussel *Dreissena polymorpha* has been widely studied in genomics, proteomics, and ecotoxicology research, with few immunohistochemical studies made of the soft tissues [26,30]. The findings of our study provide novel insights into the characterization and localization of extracellular matrix components in the soft tissues of zebra mussels. In general, the high number of positive reactions of mammalian antibodies in zebra mussels support the hypothesis that many extracellular matrix components are structurally conserved during evolution [9,12]. Furthermore, some tissue-specific recognition may provide new points of interest for relevant studies. These findings also suggest that mussels may even be a good model organism in biomedical or ecotoxicology research, especially considering the 3Rs principle (Replacement, Reduction, and Refinement) and the required reduction of vertebrate species in such research.

The expression of these extracellular matrix molecules in zebra mussel soft tissue is likely related to the specific function of tissues and organs. In the mussel soft body, the mantle epidermis secretes calcium carbonate and conchiolin to form the shell. The gills are primarily used for respiration. In mussel soft bodies, the basal lamina key component collagen IV, adhesion-related fibronectin, and crystal formation-related keratan sulfate (MZ15) antibodies are labeled in hemocytes, which implies the involvement of hemocytes in growth, immune, and mineralization processes. The foot is used for moving short distances and assembly of byssus by various specialized byssus glands. In the byssus glands, aggrecan and link protein labeling is most likely related to the mechanical function of the tissue.

In general, collagen IV, fibronectin, and keratan sulfate (detected by antibody MZ15) were all located in the cytoplasm of a subpopulation of hemocytes (the hyalinocytes-like cells, as reported in [29,31]). Our results revealed the functional heterogeneity of hemocytes with respect to the content of proteins or proteoglycans. As described in the literature, those hyalinocytes-like cells are fully capable of performing innate immune responses [29]. In previous studies, the immunolocalization of fibronectin in the subpopulations of hemocytes was reported in Pacific blue mussels (*Mytilus trossulus*) and Mediterranean mussels (*Mytilus galloprovincialis*) [32,33]. In addition, a fibronectin-like protein (with a fibronectin type III domain) was identified in zebra mussel hemolymph plasma by proteomic analysis and was observed to be upregulated during in vivo immune response [34]. Fibronectin is a high-molecular glycoprotein of the extracellular matrix which is related to cell adhesion and migration. In vertebrates, there are two types of fibronectins, the plasma-soluble fibronectin, and the insoluble cellular fibronectin. The fibronectin plays a key role in matrix assembly, wound healing, and tumor development in vivo [35]. Here our finding of fibronectin in zebra mussel hemocytes is consistent with previous studies and suggests that fibronectin may play an important role in the hemocyte-mediated immune reaction in zebra mussels.

An important function of mussel hemocytes, other than immunity, is their involvement in shell mineralization. The mechanism of shell formation has been studied for a long time and two concurrent principles have been proposed, one is the matrix-mediated hypothesis, another is the cell-mediated hypothesis [36,37]. The traditional matrix-mediated hypothesis was mainly supported by in vitro experiments, indicating that the matrix proteins have some mineralization-inducing effect. Still, the effect of matrix proteins in whole shell formation and mineralization has remained questionable. The cell-mediated hypothesis was supported by recent reports of crystal-carrying hemocytes observed in circulation and in the extrapallial space in mollusks, which indicated the potential involvement of hemocytes in shell biomineralization [38,39].

Other than the reports of crystal-carrying hemocytes, the gene expressions of shell matrix proteins in hemocytes were very low, which led to the need for additional evidence [39]. A previous study had identified a fibronectin type III domain and an alpha 1 type IV collagen in the acid-soluble matrix extract and acid-insoluble matrix of the zebra mussel shell matrix, respectively [40]. As we also immunolocalized collagen IV and fibronectin in zebra mussel hemocytes, the participation of hemocytes in shell mineralization in zebra

mussels is likely. The distribution of positive hemocytes in the central and edge regions of mantle tissues also fit the hemocyte-mediated shell mineralization hypothesis.

Keratan sulfate has Ca^{2+} counterions and may act as a calcium reserve in eggshell production and bone mineralization in birds [41,42]. With the immunolocalization of keratan sulfate (with antibody MZ15) in zebra mussel hemocytes, we can suppose that the shell formation in mussels and avian eggs might be similar in the participation of keratan sulfate proteoglycans. In contrast, another keratan sulfate antibody 1/20/5-D-4 was negative in zebra mussel soft tissues. Since the two antibodies recognize different epitopes, we have to note that only the epitope recognized by antibody MZ15 is expressed in zebra mussel soft tissue. In this regard, it is of note that keratan sulfate-containing proteoglycans are widely distributed among species and show considerable complexity in structure, with numerous epitopes recognized by different antibodies [42]. Accordingly, keratan sulfate proteoglycans may be less conserved in evolution and thus prone to exhibit different epitopes in different species.

Apart from hemocytes, the collagen IV antibody is also specifically bound to peripheral nerves and parts of ganglions in the nervous system of zebra mussels [43]. In the previous immunohistochemical study of connective tissues in the bivalves *Pecten jacobaeus* and *Mytilus galloprovincialis*, the anti-human type IV collagen antibody recognized a subepidermal basement membrane structure [44]. This is consistent with our results in *Dreissena polymorpha* and it suggests that type IV collagen is conserved and widely distributed in multicellular organisms, even sponges [45].

Unlike most members of the collagen family, type IV collagen in vertebrates is found only in the basal lamina of tissues (epithelial, muscle fibers, blood vessels, and peripheral nerves). Basal laminae are believed to be an ancient evolutionary structure and essential in the development of metazoan species [46]. Functions of basal lamina include tissue organization, barrier and filter formation, control of material diffusion, cell adhesion, cell migration, and axon outgrowth. Here, our study provides immunohistochemical evidence for the existence of basal lamina major component collagen IV and laminin (broadly positive) in the peripheral nervous system of zebra mussels. In the peripheral nervous system of vertebrates (especially mammals), axons are wrapped by a myelin sheath which is formed by Schwann cells (i.e., peripheral glia) and surrounded by a basal lamina [47]. In the vertebrate, collagen IV is not only a major component of the Schwann cell basement membrane but is also connected with various functions in the regulation of Schwann cells, promoting peripheral axonal growth and myelination [48]. Our results suggest that certain cells, perhaps comparable to Schwann cells, in the zebra mussel peripheral nervous system express collagen IV. However, it is interesting that, unlike vertebrates, there would be no collagen IV-positive basal lamina surrounding the muscle fibers, although some positive hemocytes were also present in the muscle.

In the vertebrate extracellular matrix, aggrecan and link protein are usually associated with load-bearing structures, such as articular cartilage and specific parts of the intervertebral discs. The aggregates formed by proteoglycan (mainly aggrecan), hyaluronan, and link protein can form a hydrated gel structure, with the collagen framework restricting the movement of hydrated aggrecan complexes, allowing the tissues to resist compression [49]. Other than the compressive loading, the proteoglycans in tendons (mainly aggrecan and versican) and their aggregate with hyaluronan provide tendon tissue with the capacity to resist physical stress [50].

Byssus is a bundle of filaments secreted by mussels for anchoring, including the adhesive plaque, stiff distal thread, elastic proximal thread, and stem [51]. The formation of byssus is initiated by byssus-secreting glands (stem gland, collagen gland, accessory gland, and phenol gland), in which the byssus proteins are synthesized and reserved for secretion. The specific labeling of aggrecan and link protein antibodies in byssus gland cells (with the proximal stem gland most significant) of zebra mussels may be related to the physical properties of these structures.

There are two possibilities for the function of the aggrecan and link protein expressed in byssus glands. The first possibility is that they may participate in the assembling process of the byssus matrix, especially in the byssus stem and proximal part of the byssus. In previous ultrastructural studies of those byssus glands, numerous secretory granules were observed in gland cells [52,53]. A study of the secretory granules suggested that proteins or glycoproteins seem to be the major constituent. Additionally, a common constitution of byssus was revealed, with organized filaments embedded in an amorphous matrix. The pattern of filament organization and quantity of matrix differed in regions with a higher ratio of matrix proteins in the proximal byssus [54]. The distribution of the amorphous matrix component in byssus is consistent with our immunolocalization results for aggrecan and link protein, showing a significant positive staining in the proximal byssus stem glands and less positive staining in the distal glands. It is intriguing to note that this is very similar to the principle of vertebrate insertional fibrocartilage formation [55]. Here, we suppose that aggrecan and link protein may participate in the constitution of the byssus matrix. The second possibility is that the aggrecan and link protein in the stem gland act as a connection between the byssus stem and retractor muscle, providing load-bearing capacities to tissues, as in the tendon [50].

Other than the byssus gland, the extracellular matrix molecules (aggrecan, link protein, chondroitin-4-sulfate, and dermatan sulfate (2B6, pre-digested with chondroitinase ABC and AC)) were also located in the lamina propria of the stomach and intestine. This suggests that these stress-bearing molecules may be necessary for the physical strength of the stomach and intestine lamina propria. A specific subepithelial region with mainly fibrous cells in the distal foot was labeled with the collagen XVIII antibody. During mussel adhesion, the foot attaches to the object by this region with the plaque gland secreting adhesion proteins meanwhile. The presence of collagen XVIII in this region might be related to the structural supporting abilities of collagen XVIII, which so far has been described as a heparan sulfate proteoglycan expressed in the basement membranes of vertebrates [56].

Laminin plays an important role in the formation and maintenance of basement membrane structure and characteristics, as well as the regulation of several biological functions (cell adhesion, migration, differentiation, etc.) [57]. In a previous immunohistochemical study of connective tissues in the bivalves *Pecten jacobaeus* and *Mytilus galloprovincialis*, laminin 1 also was recognized within a subepidermal basement membrane structure [44]. Decorin, which is a dermatan sulfate containing proteoglycan, may play an antagonistic role in prohibiting biomineralization within zebra mussel soft tissues, for in the eggshell biomineralization model, a 200 kDa dermatan sulfate proteoglycan had been extracted from the eggshell and was verified with concentration-dependent crystal morphology-modulating abilities in vitro [58].

It is worth noting that the labeling for CB-1 (originally designed to recognize a chicken antigen) and DS1 (directed towards a bovine antigen) showed minor intensity variation in certain zebra mussel soft tissues. The initial publication of CB-1 stated that the CB-1 antibody could not react with mammalian samples and supposed a potential structural difference in the core proteins of avian and mammalian PG-II (decorin) [59]. In our study, both epitopes of avian and mammalian (bovine) decorin were recognized in zebra mussel soft tissues, indicating that mussels could be closer to the evolutionary origin of decorin in the early stages of development.

Osteonectin (SPARC) is a non-collagenous component in bone tissue regulating osteoblast and osteoclast activities. In the mineralization of zebra mussels, so far, no specific mineralization cells, such as osteoclasts or osteoblasts, have been reported, but the mantle cells seem to possess some of the capabilities of these vertebrate bone cells. The broadly expressed pattern of SPARC in zebra mussel soft tissues was also consistent with the report of gene expression of collagen IV and SPARC in oyster tissues [8]. SPARC expression in mussels might regulate the formation and growth of mineral crystals, cell–cell and cell–matrix interactions, and inhibition of cell migration [60], which is also important for immune responses.

5. Conclusions

In the present study, an immunohistochemical labeling strategy for extracellular matrix molecules in zebra mussel soft tissues was established. Furthermore, the presence of collagen IV, fibronectin, and keratan sulfate epitopes in hemocytes was reported, as well as the presence of collagen IV in peripheral nerves, aggrecan and link protein in byssus glands, collagen XVIII in distal foot, and a broader occurrence of laminin, osteonectin, and decorin in mussel soft tissues. The results support the cell-mediated shell formation hypothesis, hemocyte-mediated immune reaction, and provide evidence for some associated molecules in peripheral nerves and byssus formation in zebra mussels. Furthermore, the results confirm that certain extracellular matrix molecules seem to be well conserved during evolution. This means that the zebra mussel constitutes a promising model that can be used in biochemistry, molecular biology, ecotoxicology research, and research focusing on the stimulation and disturbance of bio-mineralization instead of conventional vertebrate models.

Author Contributions: Conceptualization, C.S. and S.M.; methodology, C.S. and S.M.; software, S.M.; validation, W.W. and S.M.; formal analysis, W.W. and S.M.; investigation, W.W.; resources, C.S.; data curation, W.W.; writing—original draft preparation, W.W.; writing—review and editing, W.W., C.S., S.M., K.S., S.B. and J.G.; visualization, W.W.; supervision, C.S.; project administration, C.S. and S.M.; funding acquisition, C.S. and W.W. All authors have read and agreed to the published version of the manuscript.

Funding: This research was funded by the China Scholarship Council (CSC), grant number no. 201808500132. The funding source had no involvement in the conduct of this study or submission for publication.

Institutional Review Board Statement: All experiments in this study were performed according to German animal protection regulations which do not require registration or approval of experiments using zebra mussels.

Data Availability Statement: The datasets used and analyzed in this study are available from the corresponding author on reasonable request.

Acknowledgments: The monoclonal antibodies M3F7 developed by H. Furthmayr, 6C4 by W.M. Halfter, MZ15 by F.M. Watt, DS1 by A.R. Poole, CB-1 by D.A. Carrino, HFN 7.1 by R.J. Klebe, 12/21/1-C-6, 9/30/8-A-4 by B. Caterson, and AON-1 by J.D. Termine, were obtained from the Developmental Studies Hybridoma Bank, created by the NICHD of the NIH and maintained at the University of Iowa, Department of Biology, Iowa City, IA 52242. Antibodies 2B6, 3B3,1/20/5-D-4 were gifts from B. Caterson. The authors thank Andrea Haderer, Claudia Harbauer, Beate Aschauer, Barbara Mosler, and Astrid Baltruschat for expert technical assistance.

Conflicts of Interest: The authors declare no conflict of interest.

References

1. Rosenberg, G. A New Critical Estimate of Named Species-Level Diversity of the Recent Mollusca. *Am. Malacol. Bull.* **2014**, *32*, 308. [CrossRef]
2. Lummer, E.-M.; Auerswald, K.; Geist, J. Fine sediment as environmental stressor affecting freshwater mussel behavior and ecosystem services. *Sci. Total Environ.* **2016**, *571*, 1340–1348. [CrossRef] [PubMed]
3. Vaughn, C.C. Ecosystem services provided by freshwater mussels. *Hydrobiologia* **2018**, *810*, 15–27. [CrossRef]
4. Hartmann, J.T.; Beggel, S.; Auerswald, K.; Stoeckle, B.C.; Geist, J. Establishing mussel behavior as a biomarker in ecotoxicology. *Aquat. Toxicol.* **2016**, *170*, 279–288. [CrossRef] [PubMed]
5. Boeker, C.; Lueders, T.; Mueller, M.; Pander, J.; Geist, J. Alteration of physico-chemical and microbial properties in freshwater substrates by burrowing invertebrates. *Limnologica* **2016**, *59*, 131–139. [CrossRef]
6. Zuykov, M.; Pelletier, E.; Harper, D.A.T. Bivalve mollusks in metal pollution studies: From bioaccumulation to biomonitoring. *Chemosphere* **2013**, *93*, 201–208. [CrossRef]
7. Li, J.; Lusher, A.L.; Rotchell, J.M.; Deudero, S.; Turra, A.; Bråte, I.L.N.; Sun, C.; Shahadat Hossain, M.; Li, Q.; Kolandhasamy, P.; et al. Using mussel as a global bioindicator of coastal microplastic pollution. *Environ. Pollut.* **2019**, *244*, 522–533. [CrossRef]
8. Dyachuk, V. Extracellular matrix components in bivalvia: Shell and ECM components in developmental and adult tissues. *Fish Aquac. J.* **2018**, *9*, 1000248. [CrossRef]

9. Brown, N.H. Extracellular matrix in development: Insights from mechanisms conserved between invertebrates and vertebrates. *Cold Spring Harb. Perspect. Biol.* **2011**, *3*, a005082. [CrossRef]
10. Theocharis, A.D.; Skandalis, S.S.; Gialeli, C.; Karamanos, N.K. Extracellular matrix structure. *Adv. Drug Deliv. Rev.* **2016**, *97*, 4–27. [CrossRef]
11. Tanzer, M.L. Current concepts of extracellular matrix. *J. Orthop. Sci.* **2006**, *11*, 326–331. [CrossRef] [PubMed]
12. Ozbek, S.; Balasubramanian, P.G.; Chiquet-Ehrismann, R.; Tucker, R.P.; Adams, J.C. The evolution of extracellular matrix. *Mol. Biol. Cell* **2010**, *21*, 4300–4305. [CrossRef] [PubMed]
13. Matsushiro, A.; Miyashita, T. Evolution of hard-tissue mineralization: Comparison of the inner skeletal system and the outer shell system. *J. Bone Miner. Metab.* **2004**, *22*, 163–169. [CrossRef] [PubMed]
14. Marzocchi, U.; Bonaglia, S.; Zaiko, A.; Quero, G.M.; Vybernaite-Lubiene, I.; Politi, T.; Samuiloviene, A.; Zilius, M.; Bartoli, M.; Cardini, U. Zebra Mussel Holobionts Fix and Recycle Nitrogen in Lagoon Sediments. *Front. Microbiol.* **2020**, *11*, 610269. [CrossRef] [PubMed]
15. Prud'homme, S.M.; Hani, Y.M.I.; Cox, N.; Lippens, G.; Nuzillard, J.-M.; Geffard, A. The zebra mussel (*Dreissena polymorpha*) as a model organism for ecotoxicological studies: A prior ^{1}H NMR Spectrum Interpretation of a Whole Body Extract for Metabolism Monitoring. *Metabolites* **2020**, *10*, 256. [CrossRef]
16. Viarengo, A.; Canesi, L. Mussels as biological indicators of pollution. *Aquaculture* **1991**, *94*, 225–243. [CrossRef]
17. Sternecker, K.; Geist, J.; Beggel, S.; Dietz-Laursonn, K.; de La Fuente, M.; Frank, H.-G.; Furia, J.P.; Milz, S.; Schmitz, C. Exposure of zebra mussels to extracorporeal shock waves demonstrates formation of new mineralized tissue inside and outside the focus zone. *Biol. Open* **2018**, *7*, bio033258. [CrossRef]
18. Wu, W.; Maffulli, N.; Furia, J.P.; Meindlhumer, L.; Sternecker, K.; Milz, S.; Schmitz, C. Exposure of zebra mussels to radial extracorporeal shock waves: Implications for treatment of fracture nonunions. *J. Orthop. Surg. Res.* **2021**, *16*, 707. [CrossRef]
19. Kertzman, P.; Császár, N.B.M.; Furia, J.P.; Schmitz, C. Radial extracorporeal shock wave therapy is efficient and safe in the treatment of fracture nonunions of superficial bones: A retrospective case series. *J. Orthop. Surg. Res.* **2017**, *12*, 164. [CrossRef]
20. Liu, F.; Reichl, F.-X.; Milz, S.; Wölfle, U.C.; Kühnisch, J.; Schmitz, C.; Geist, J.; Hickel, R.; Högg, C.; Sternecker, K. Disrupted biomineralization in zebra mussels after exposure to bisphenol-A: Potential implications for molar-incisor hypomineralization. *Dent. Mater.* **2022**. *ahead of print*. [CrossRef]
21. Titorencu, I.; Pruna, V.; Jinga, V.V.; Simionescu, M. Osteoblast ontogeny and implications for bone pathology: An overview. *Cell Tissue Res.* **2014**, *355*, 23–33. [CrossRef] [PubMed]
22. Kylmaoja, E.; Nakamura, M.; Tuukkanen, J. Osteoclasts and remodeling based bone formation. *Curr. Stem Cell Res. Ther.* **2016**, *11*, 626–633. [CrossRef] [PubMed]
23. American Society of Testing and Materials (ASTM). Standard Guide for Conducting Laboratory Toxicity Tests with Freshwater Mussels. In *Annual Book of ASTM Standards*; ASTM International: West Conshohocken, PA, USA, 2013; p. 52.
24. Sicuro, B. Freshwater bivalves rearing: A brief overview. *Int. Aquat. Res.* **2015**, *7*, 93–100. [CrossRef]
25. Bignell, J.P.; Stentiford, G.D.; Taylor, N.G.H.; Lyons, B.P. Histopathology of mussels (*Mytilus* sp.) from the Tamar estuary, UK. *Mar. Environ. Res.* **2011**, *72*, 25–32. [CrossRef] [PubMed]
26. Morton, B. Chapter 12 The Anatomy of *Dreissena polymorpha* and the Evolution and Success of the Heteromyarian Form in the Dreissenoidea. In *Zebra Mussels: Biology, Impacts, and Control*, 1st ed.; Nalepa, T.F., Schloesser, D.W., Eds.; Lewis Publishers: Boca Raton, FL, USA, 1993; pp. 185–215.
27. Milz, S.; Regner, F.; Putz, R.; Benjamin, M. Expression of a wide range of extracellular matrix molecules in the tendon and trochlea of the human superior oblique muscle. *Investig. Ophthalmol. Vis. Sci.* **2002**, *43*, 1330–1334.
28. Carballal, M.J.; López, C.; Azevedo, C.; Villalba, A. Enzymes involved in defense functions of hemocytes of mussel *Mytilus galloprovincialis*. *J. Invertebr. Pathol.* **1997**, *70*, 96–105. [CrossRef]
29. Evariste, L.; Auffret, M.; Audonnet, S.; Geffard, A.; David, E.; Brousseau, P.; Fournier, M.; Betoulle, S. Functional features of hemocyte subpopulations of the invasive mollusk species *Dreissena polymorpha*. *Fish Shellfish Immunol.* **2016**, *56*, 144–154. [CrossRef]
30. Beggel, S.; Cerwenka, A.; Brandner, J.; Geist, J. Shell morphological versus genetic identification of quagga mussel (*Dreissena bugensis*) and zebra mussel (*Dreissena polymorpha*). *Aquat. Invas.* **2015**, *10*, 93–99. [CrossRef]
31. Beggel, S.; Hinzmann, M.; Machado, J.; Geist, J. Combined impact of acute exposure to ammonia and temperature stress on the freshwater mussel *Unio pictorum*. *Water* **2017**, *9*, 455. [CrossRef]
32. Panara, F.; Di Rosa, I.; Fagotti, A.; Simoncelli, F.; Mangiabene, C.; Pipe, R.K.; Pascolini, R. Characterization and immunocytochemical localization of actin and fibronectin in haemocytes of the mussel *Mytilus galloprovincialis*. *Histochem. J.* **1996**, *28*, 123–131. [CrossRef]
33. Dyachuk, V.A.; Maiorova, M.A.; Odintsova, N.A. Identification of β integrin-like- and fibronectin-like proteins in the bivalve mollusk *Mytilus trossulus*. *Dev. Growth Differ.* **2015**, *57*, 515–528. [CrossRef] [PubMed]
34. Leprêtre, M.; Almunia, C.; Armengaud, J.; Le Guernic, A.; Salvador, A.; Geffard, A.; Palos-Ladeiro, M. Identification of immune-related proteins of *Dreissena polymorpha* hemocytes and plasma involved in host-microbe interactions by differential proteomics. *Sci. Rep.* **2020**, *10*, 6226. [CrossRef] [PubMed]
35. Patten, J.; Wang, K. Fibronectin in development and wound healing. *Adv. Drug Deliv. Rev.* **2021**, *170*, 353–368. [CrossRef] [PubMed]

36. Song, X.; Liu, Z.; Wang, L.; Song, L. Recent advances of shell matrix proteins and cellular orchestration in marine molluscan shell biomineralization. *Front. Mar. Sci.* **2019**, *6*, 41. [CrossRef]
37. Addadi, L.; Joester, D.; Nudelman, F.; Weiner, S. Mollusk shell formation: A source of new concepts for understanding biomineralization processes. *Chemistry* **2006**, *12*, 980–987. [CrossRef] [PubMed]
38. Mount, A.S.; Wheeler, A.P.; Paradkar, R.P.; Snider, D. Hemocyte-mediated shell mineralization in the eastern oyster. *Science* **2004**, *304*, 297–300. [CrossRef] [PubMed]
39. Huang, J.; Li, S.; Liu, Y.; Liu, C.; Xie, L.; Zhang, R. Hemocytes in the extrapallial space of *Pinctada fucata* are involved in immunity and biomineralization. *Sci. Rep.* **2018**, *8*, 4657. [CrossRef]
40. Immel, F.; Broussard, C.; Catherinet, B.; Plasseraud, L.; Alcaraz, G.; Bundeleva, I.; Marin, F. The shell of the invasive bivalve species *Dreissena polymorpha*: Biochemical, elemental and textural investigations. *PLoS ONE* **2016**, *11*, e0154264. [CrossRef]
41. Ha, Y.W.; Son, M.J.; Yun, K.S.; Kim, Y.S. Relationship between eggshell strength and keratan sulfate of eggshell membranes. *Comp. Biochem. Physiol. A Mol. Integr. Physiol.* **2007**, *147*, 1109–1115. [CrossRef]
42. Caterson, B.; Melrose, J. Keratan sulfate, a complex glycosaminoglycan with unique functional capability. *Glycobiology* **2018**, *28*, 182–206. [CrossRef]
43. Yurchenko, O.V.; Savelieva, A.V.; Kolotuchina, N.K.; Voronezhskaya, E.E.; Dyachuk, V.A. Peripheral sensory neurons govern development of the nervous system in bivalve larvae. *Evodevo* **2019**, *10*, 22. [CrossRef] [PubMed]
44. Corbetta, S.; Bairati, A.; Vitellaro Zuccarello, L. Immunohistochemical study of subepidermal connective of molluscan integument. *Eur. J. Histochem.* **2002**, *46*, 259–272. [CrossRef] [PubMed]
45. Boute, N.; Exposito, J.-Y.; Boury-Esnault, N.; Vacelet, J.; Noro, N.; Miyazaki, K.; Yoshizato, K.; Garrone, R. Type IV collagen in sponges, the missing link in basement membrane ubiquity. *Biol. Cell* **1996**, *88*, 37–44. [CrossRef]
46. Halfter, W.; Oertle, P.; Monnier, C.A.; Camenzind, L.; Reyes-Lua, M.; Hu, H.; Candiello, J.; Labilloy, A.; Balasubramani, M.; Henrich, P.B.; et al. New concepts in basement membrane biology. *FEBS J.* **2015**, *282*, 4466–4479. [CrossRef] [PubMed]
47. Chernousov, M.A.; Yu, W.-M.; Chen, Z.-L.; Carey, D.J.; Strickland, S. Regulation of Schwann cell function by the extracellular matrix. *Glia* **2008**, *56*, 1498–1507. [CrossRef]
48. Chen, P.; Cescon, M.; Bonaldo, P. The Role of Collagens in Peripheral Nerve Myelination and Function. *Mol. Neurobiol.* **2015**, *52*, 216–225. [CrossRef]
49. Kiani, C.; Chen, L.; Wu, Y.J.; Yee, A.J.; Yang, B.B. Structure and function of aggrecan. *Cell Res.* **2002**, *12*, 19–32. [CrossRef]
50. Yoon, J.H.; Halper, J. Tendon proteoglycans: Biochemistry and function. *J. Musculoskelet. Neuronal Interact.* **2005**, *5*, 22–34.
51. Coyne, K.J.; Qin, X.X.; Waite, J.H. Extensible collagen in mussel byssus: A natural block copolymer. *Science* **1997**, *277*, 1830–1832. [CrossRef]
52. Tamarin, A. An ultrastructural study of byssus stem formation in *Mytilus californianus*. *J. Morphol.* **1975**, *145*, 151–177. [CrossRef]
53. Zuccarello, L.V. The collagen gland of *Mytilus galloprovincialis*: An ultrastructural and cytochemical study on secretory granules. *J. Ultrastruct. Res.* **1980**, *73*, 135–147. [CrossRef]
54. Golser, A.; Scheibel, T. Routes towards Novel Collagen-Like Biomaterials. *Fibers* **2018**, *6*, 21. [CrossRef]
55. Chatuparisute, P.; Shinohara, Y.; Kirchhoff, C.; Fischer, F.; Milz, S. Immunohistochemical composition of the human lunotriquetral interosseous ligament. *Appl. Immunohistochem. Mol. Morphol.* **2012**, *20*, 318–324. [CrossRef] [PubMed]
56. Seppinen, L.; Pihlajaniemi, T. The multiple functions of collagen XVIII in development and disease. *Matrix Biol.* **2011**, *30*, 83–92. [CrossRef]
57. Barros, D.; Amaral, I.F.; Pêgo, A.P. Laminin-inspired cell-instructive microenvironments for neural stem cells. *Biomacromolecules* **2020**, *21*, 276–293. [CrossRef]
58. Carrino, D.A.; Dennis, J.E.; Wu, T.M.; Arias, J.L.; Fernandez, M.S.; Rodriguez, J.P.; Fink, D.J.; Heuer, A.H.; Caplan, A.I. The avian eggshell extracellular matrix as a model for biomineralization. *Connect. Tissue Res.* **1996**, *35*, 325–329. [CrossRef]
59. Lennon, D.P.; Carrino, D.A.; Baber, M.A.; Caplan, A.I. Generation of a monoclonal antibody against avian small dermatan sulfate proteoglycan: Immunolocalization and tissue distribution of PG-II (Decorin) in embryonic tissues. *Matrix* **1991**, *11*, 412–427. [CrossRef]
60. Rosset, E.M.; Bradshaw, A.D. SPARC/osteonectin in mineralized tissue. *Matrix Biol.* **2016**, *52–54*, 78–87. [CrossRef]

4. Discussion

4.1 New shell mineralization induced by radial extracorporeal shock waves in zebra mussels

In the first paper, we explored the shell mineralization of zebra mussels after treatments of radial ESWT at different energy levels. Similar to the previous study of focused ESWT, significant rESW-induced mineralization was observed in several groups. Other than that, a dose-dependent biomineralization effect could be concluded from the results of rESWT exposure experiments.

4.1.1 Radial extracorporeal shock waves can induce biomineralization in the shell

An invertebrate animal model of biomineralization was established using zebra mussels and verified with the treatment of focused ESWs [12]. The zebra mussels treated by focused ESWs in water showed a significantly higher mean fluorescence intensity in the shell mineralization zone than the sham-exposed group. Besides, the study also demonstrated that the biomineralization induced by fESWs in mussel shells might not be restricted to the region with the highest energy density. The fESW-induced shell biomineralization concentrated on the region close to the umbo, representing the physiological mineralization process of mussel shells. Here in the first paper, the mineralization inducing ability of rESWT was verified with significantly higher mean fluorescence intensities in the radial ESWT treated groups than in the sham-exposed group using the zebra mussel as a novel biomineralization animal model.

The distribution of new mineralization in the shell exhibited a similar pattern as reported in Sternecker et al. [12]. Unlike our previous study, the fluorescence intensity between left and right valves showed a significant difference. In most groups, the left valve (target side) showed a higher fluorescence intensity than the right valve. This difference between left and right valves may be caused by the relatively low energy level and the narrow region of effect (i.e., of biological efficacy) for rESWT devices (region size less than 15*20mm) [13]. In the fESWT study, the EFD at the focus point was about 0.4 mJ/mm2 with a deep effective region (about 20*50mm) that can cover the whole mussel. In this case, the whole mussel (including the soft body and the shells) can be impacted by the fESWs.

The fESWs may trigger some biological mineralization processes in the mussel and lead to similar mineralization in both valves [12]. While in the present rESWT study, the highest EFD on the target point was about 0.11 mJ/mm2 with a narrow effective region (less than 15*20mm) that could not cover the whole mussel [14]. In this case, the rESWT might trigger only the mineralization process in the targeted left valve and adjacent epitheliums but not in the whole soft tissues, e.g., the hemocytes-mediated shell formation [11].

In an experiment with rabbit femurs exposed to ESWT, a similar pattern of ESW-induced new mineralization as in our study was reported with the new bone formation being presented and increased with the rise of ESW energy (with 0.5, 0.9, and 1.2 mJ/mm2 EFD). It was interesting to note that in the highest energy level (1.2 mJ/mm2 EFD), ESWT resulted in a new bone formation on the dorsal side (not treated side) of the rabbit femur which was consistent with our results in mussels (4 bar caused a significant increase of fluorescence intensity in the not treated right side of shells) [43]. The presence of new mineralization outside the ESW targeted region indicated that the ESW-induced new mineralization was conducted not directly by the mechanical waves but was mediated by certain biological activities among the targeted region of tissues. In mammals, the biological activities induced by ESWT contain the expressions of biomolecules of osteogenesis (BMP-2, RUNX2, Osteocalcin) and angiogenesis (VEGF, eNOS, PCNA) at the gene or molecular levels, while the biological reactions in mussels remained unknown [29, 68]. However, because of the significant differences between the tissue organization in vertebrates and invertebrates, the next important thing to do is to explore the ECM composition of zebra mussel soft bodies.

To investigate whether ECM molecules in mussel soft tissues exist, which may be related to the ESW-induced biomineralization, we conducted an immunohistochemical detection of some human ECM molecules in zebra mussel soft tissues in my second paper.

4.1.2 The shell biomineralization induced by radial extracorporeal shock waves has a dose-effect relationship

As presented in the first paper, the mean fluorescence intensity on the left shells showed a rising trend as the energy went up, which could be interpreted as a

dose-dependent increase in biomineralization induced by rESWT. The dose-effect relationship was also supported by the statistical results. In the results of targeted left shells, those groups with different energy levels could be divided into three stages: In sham exposure and 2 bar groups, left shells showed very low fluorescence intensity. In 2.5 bar, 3 bar, and 3.5 bar groups, left shells showed significantly higher fluorescence intensity than sham exposure and 2 bar groups. In the 4 bar group, left shells showed significantly higher fluorescence intensity than all the other groups. Similar results could be found in the periosteal ventral side of the rabbit femur in a focused ESWT study, showing the 0 and 0.35 mJ/mm2 EFD groups with no new bone formation, the 0.5, 0.9, and 1.2 mJ/mm2 EFD groups with significant new bone formation than the sham exposure group. The amount of new bone formation also increased with increasing EFD (0.5, 0.9, and 1.2 mJ/mm2) [43]. Besides, a study in rabbits focused on the milestones of biological mineralization post certain low energy rESWTs (4000 impulses with EFD 0.16 mJ/mm²) and reported that the rESW-induced new bone formation presented in all groups, with the highest intensity of ossification after four weeks [44]. Those studies have described a dose-dependent, time-limited biomineralization effect induced by rESWT in vivo.

It is interesting to note that the unexposed right valve showed relatively low fluorescence intensity in most groups, with the exception of the 4 bar group. It fits our hypothesis that the higher EFD of ESWs may trigger some biomineralization process within the soft body resulting in the mineralization in both shells [12].

The aquatic environment of mussels is a homogeneous medium in which the propagation path of ESWs can be visualized, and the distribution of ESWs energy can be measured [13, 14]. It makes the zebra mussel suitable for ESWT studies as an invertebrate biomineralization animal model. However, the mechanisms of ESW-induced shell mineralization remain uncertain at molecule and cell levels. In the second paper, an immunohistochemical study was conducted to investigate the mineralization-related ECM molecules in zebra mussel soft tissues.

4.2 The immunodetection of extracellular matrix components in zebra mussel soft tissues

In the second paper, we report an immunohistochemical detection of the ECM components of zebra mussel soft tissues using a panel of well-characterized monoclonal antibodies. These antibodies were made against collagen, proteoglycans, glycosaminoglycans, and glycoproteins. All of them have been demonstrated in mammalian ECM tissues [69-71]. The distance between the zebra mussel and mammals is far in the evolutionary path, and the composition of the ECM in mussels could be quite different from the mammals. Still, several studies have demonstrated the presence of the same or similar matrix molecules in the ECM of bivalve mussels as in mammals [72-74]. We hypothesize that some ECM molecules (or at least molecule fragments, i.e., epitopes) are conserved in evolution, and some molecules might be detected using anti-mammal monoclonal antibodies. The potential ECM molecules shared by mammals and mussels might bring us a better understanding of the biological activities in bivalve soft tissues and support our related studies using the zebra mussel as an animal model. In particular, we tested some antibodies previously related to biological mineralization.

4.2.1 Collagen IV, fibronectin, keratan sulfate (MZ15 - epitope) in zebra mussel hemocytes

Among all structures of mussel soft tissues, the hemolymph is not only responsible for nutrient transport, growth, and development but also a major component of the immune system. A study on zebra mussel hemocytes has observed and classified subpopulations of hemocytes and demonstrated that hyalinocytes and granulocytes have full innate immunity [75]. It is worth noting that the antibodies recognizing collagen IV, fibronectin, and keratan sulfate (MZ15 - epitope) all labeled a subpopulation of mussel hemocytes specifically. According to the classification of Evariste et al. [75], those positive hemocytes could be recognized as hyalinocytes-like hemocytes.

The presence of collagen IV, fibronectin, and keratan sulfate in hemocytes could be related to various functions mediated by mussel hemocytes, such as nutrient transport, tissue development, wound healing, immune reactions, and hemocytes mediated biomineralization [76-78]. Although few studies have explored the presence of mammal ECM molecules in bivalves, some pieces of evidence were

found to be helpful in publications. A study had identified a fibronectin type III domain and an alpha 1 type IV collagen in the acid-soluble matrix extract and acid-insoluble matrix of zebra mussel shell matrix, respectively, suggesting that they may participate in the formation of the shell [79]. As we also immunolocalized collagen IV and fibronectin in zebra mussel hemocytes, the participation of hemocytes in shell mineralization in zebra mussels is likely. Keratan sulfate has Ca2+ counterions, and it may act as a calcium reserve in eggshell production and bone mineralization in birds [80, 81]. The detection of keratan sulfate in mussel hemocytes indicates that it may act as a calcium reserve in hemocytes during the hemocyte-mediated shell mineralization.

Some published studies have also immunolocalized fibronectin in the subpopulation of hemocytes in marine mussels *Mytilus trossulus* and *Mytilus galloprovincialis* [82, 83]. Thus, our results in freshwater mussels are not too surprising. In a previous immunohistochemical study of connective tissues in bivalve *Pecten jacobaeus* and *Mytilus galloprovincialis*, the anti-human type IV collagen antibody recognized a subepidermal basement membrane structure [74]. These saltwater animal studies are consistent with our reports of the presence of collagen IV, fibronectin, and keratan sulfate in freshwater zebra mussel hemocytes. Besides, the distribution of positive staining hemocytes in the mantle and inter mantle space also supports the hemocytes-mediated shell mineralization hypothesis [62, 84, 85].

In a study of the avian eggshell matrix, several epitopes of keratan sulfate were detected in different regions of the eggshell membrane and shell itself, with the content being proportional to eggshell stability [55, 80]. Subsequent studies revealed the functions of different keratan sulfate proteoglycans (osteoadherin, fibromodulin, etc.) in which the keratan sulfate may act as calcium reservoirs in the eggshell assembly, bone formation, and the production of action potentials in neurons [81]. Considering the immunolocalization of keratan sulfate (with antibody MZ15) in zebra mussel hemocytes and the hemocyte mediated shell mineralization hypothesis, we can suppose that the keratan sulfate proteoglycans might act as calcium reserve within hemocytes during the shell formation in mussels just as in the avian eggs. It is worth noting that another keratan sulfate antibody 1/20/5-D-4, which recognizes a different epitope on the keratan sulfate mac-

romolecule, was negative in zebra mussel soft tissues. The keratan sulfate-containing proteoglycans are widely distributed among species with numerous epitopes recognized by different antibodies [81]. Since the two antibodies recognize different epitopes in our experiments, we need to note that only the epitope recognized by antibody MZ15 is expressed in the hemocytes of zebra mussels.

4.2.2 Collagen IV in the peripheral nervous system

Other than the hemocytes, the peripheral nerves and parts of ganglions in zebra mussels also showed positive labeling by the anti-human type IV collagen antibodies. Human type IV collagen has been immunodetected in a subepidermal basement membrane structure of other bivalve mussels (*Pecten jacobaeus* and *Mytilus galloprovincialis*), demonstrating that it is conserved in the evolutionary process [74]. Here our results demonstrated the presence of type IV collagen in the peripheral nervous system of zebra mussels. This is consistent with previous studies showing the presence of type IV collagen in bivalve mussel tissues and provides new evidence for the existence of type IV collagen in the mussel peripheral nerve system.

In vertebrates, type IV collagen is located mainly in the basal lamina of various tissues (epithelial, muscle fibers, blood vessels, and peripheral nerves). Functions of collagen IV in the basal lamina include tissue organization, barrier and filter formation, control of material diffusion, cell adhesion, cell migration, and axon outgrowth. In the peripheral nervous system of vertebrates, axons are wrapped by a myelin sheath (of varying thickness) which is formed by Schwann cells and surrounded by a basal lamina [86]. Collagen IV is known to be not only a major component of the Schwann cell basement membrane but also connected with various functions such as the regulation of Schwann cell growth, promoting peripheral axonal growth, and myelination [87]. Our results suggest that certain cells, perhaps comparable to Schwann cells, in the zebra mussel peripheral nervous system express collagen IV. This may provide clues to the genesis and development of the shellfish nervous system.

4.2.3 Aggrecan and link protein in the byssus glands

Aggrecan and link protein are located mainly in some load-bearing structures such as the articular cartilage and intervertebral disc. The aggregates formed by

proteoglycan (mainly aggrecan), hyaluronan, and link protein endow articular cartilage or intervertebral disc with its ability to withstand compressive loads [88]. Alternatively, in fibrocartilaginous tendon tissue, the proteoglycans (mainly aggrecan and versican) and hyaluronan provide tendon tissue with the capacity to resist compressive and tensile forces [89].

In order to adhere to solid surfaces, mussels produce the byssus, which is a bundle of filaments secreted by the foot, consisting of the adhesive plaque, stiff distal thread, elastic proximal thread, and stem [90]. The byssus is secreted by byssus-secreting glands (including stem gland, collagen gland, accessory gland, and phenol gland), in which the byssus proteins are synthesized and reserved for secretion. The immunolabeling of aggrecan and link protein antibodies in byssus glands suggests that aggrecan and link protein might be involved in the byssus formation and contribute to the physical properties of the byssus.

It is worth noting that the constituent molecules of byssus are still unclear. Therefore, we hypothesize that there are two possibilities regarding the role of aggrecan and link proteins expressed in byssus glands. The first possibility is that aggrecan and link proteins may participate in the assembling process of the byssus matrix, especially in the byssus stem and proximal part of the byssus. In the ultrastructural studies of byssus glands, numerous secretory granules consisting of proteins or glycoproteins were observed in gland cells [91, 92]. The aggrecan and link protein may locate in those secretory granules and participate in the construction of the amorphous matrix of the byssus. Specifically, the proportion of the amorphous matrix in the byssus was higher in the proximal and lower in distal parts, which is consistent with our immunostaining results showing significant positive staining in the proximal byssus stem glands and less positive staining in distal glands [93]. It is worth noting that this composing pattern of byssus is strikingly similar to the principle of insertional fibrocartilage formation in vertebrates [70, 94]. The second possibility is that aggrecan and link proteins in the stem glands may provide the gland cells a capacity to resist tensile and compressive stress as in the tendon so that the byssus stem generator (containing stem gland cells) could act as a connection between the muscle fibers and byssus stem filaments [89, 91].

4.2.4 Other extracellular matrix molecules located in the zebra mussel soft tissues

The unspecific labeling of laminin, decorin (DS1 and CB-1), and osteonectin in zebra mussel soft tissues also showed the conservation of those molecules during evolution. Laminin is a large molecular weight glycoprotein composed of many distinct domains with different structures and functions. It plays an vital role in the formation and maintenance of the basement membrane, regulation of cell adhesion, migration, and differentiation [95]. A previous immunohistochemical study had immunolocalized laminin 1 in a subepidermal basement membrane structure of bivalves *Pecten jacobaeus* and *Mytilus galloprovincialis* [74]. Our study repeated the immunodetection of laminin in bivalve mussels. The results confirmed the existence of laminin epitopes in zebra mussel soft tissues, showing that laminin might be important in tissue organization in bivalves.

Decorin is a dermatan sulfate-containing ECM proteoglycan that is involved in the regulation of autophagy, endothelial cell behavior, and inhibition of angiogenesis in vertebrates [96, 97]. In a study of eggshell bio-mineralization, a 200-kDa dermatan sulfate proteoglycan was extracted from the eggshell and was verified with concentration-dependent crystal morphology modulating abilities in vitro [55]. The broadly positive labeling of CB-1 and DS1 antibodies in zebra mussel soft tissues indicates that it may be related to prohibiting biomineralization within zebra mussel soft tissues. The anti- decorin antibodies DS1 and CB-1 were made to recognize antigens in bovine and chicken, respectively. Besides, the initial publication using CB-1 antibody supposed potential structural differences in the core proteins of avian and mammalian PG-II (decorin) [98]. In comparison, both CB-1 and DS1 anti-bodies reacted with zebra mussel soft tissues in our results, indicating that both epitopes of avian (chicken) and mammalian (bovine) decorin were expressed in zebra mussel tissues, and the mussels might be closer to the evolutionary origin of decorin in the early stages of development.

Osteonectin (SPARC) is secreted by osteoblasts in the bone of vertebrates, and the levels of SPARC are associated with the mineralization of collagen [56]. During the mineralization of zebra mussels, so far, no specific mineralization cells such as osteoblasts have been reported. However, in the cell-mediated shell mineralization hypothesis, the mantle cells seem to be involved in some processes of calcium carbonate mineralization which makes this function comparable to that

of vertebrate bone cells [63]. The broad expression of SPARC in zebra mussel tissues indicates that SPARC may act as a regulator of mineral crystal formation, growth, and remodeling, as reported in vertebrates [99].

In addition, the lamina propria of the stomach and intestine were labeled with antibodies against aggrecan, link protein, chondroitin-4-sulfate, and dermatan sulfate (antibody 2B6, tissue pre-digested with chondroitinase ABC and AC), a specific subepithelial region with mainly fibrous cells in the distal foot was labeled with a collagen XVIII antibody. The expression of these structural supporting ECM molecules in the lamina propria and distal foot region might contribute to the physical strength required in these tissues [88, 100, 101].

5. Summary

It has been decades since extracorporeal shock wave treatment (ESWT) was applied to treat bone lesions. However, the physical-biological mechanism of the ESW-induced biomineralization process is still unclear. We used a newly developed mussel animal model to study the biomineralization-inducing effect of rESWT and the dose-effect relationship. The aquatic environment of mussels provides a homogeneous medium for the transmission of ESWs. It thus controls the shock wave energies in the dose-bioeffect relationship study of rESWT using zebra mussel as a biomineralization animal model. Other than the rESW-induced biomineralization and its dose-effect relationship, the biological mechanism of mussel shell mineralization is still unclear. Thus, an immunohistochemical study on the mineralization-related ECM molecules was also conducted on zebra mussel soft tissues.

In the first study, mussels were exposed to rESWs at different energy levels, followed by fluorescence intensity analysis of shells by region. Compared with the control groups, those mussels exposed to different energy of rESWs showed a significantly higher fluorescence intensity in some regions. The exposure of mussels in rESWT repeated the results of fESWT, which indicated that fESWT could induce new mineralization in shells. The results of mussels exposed to rESWT indicated that the rESWT could induce new mineralization in shells as that of fESWT. Besides, the results showed that the biomineralization induced by rESWT increases as the shock wave energy rises. The statistical analysis showed significant differences in the fluorescence intensity among groups, with higher energy rESWT resulting in more intensive fluorescence. Those results suggest that rESWT has dose-dependent biomineralization inducing effects with increasing biomineralization after higher energy shock waves.

In a second study, the immunohistochemical detection of extracellular matrix components in the soft tissues of zebra mussels was undertaken. Our results regarding the expression of type IV collagen, fibronectin, and keratan sulfate in zebra mussel hemocytes are consistent with the hemocytes-mediated shell formation hypothesis. The functions of type IV collagen, fibronectin, and keratan sulfate in hemocytes may be related to hemocyte-mediated biomineralization. Besides, type IV collagen was also labeled in the peripheral nervous systems

with a potential role as a basal lamina constituent. Furthermore, aggrecan and link protein expression was detected in the various byssus gland cells. In mammalian tissues, aggrecan and link protein contribute to structural stability and resistance against compressive forces. The aggrecan and link protein in mussel byssus glands might participate in the synthesis of byssus threads or contribute to the structural strength of the byssus-muscle connection. In addition, some ECM components (laminin, decorin, and osteonectin) were found to be widespread in zebra mussel tissues. They may play a role in tissue organization, prohibiting biomineralization, or as a regulator of the mineral crystals formation. Those mammal ECM molecules detected in zebra mussel soft tissues demonstrate the conservation of ECM molecules in evolution, provide supporting evidence for hemocyte mediated shell formation hypothesis, and bring up clues for further study of zebra mussels as a biomineralization related animal model.

6. Zusammenfassung

Obwohl die extrakorporale Stoßwellenbehandlung (ESWT) seit Jahrzehnten zur Behandlung von Knochenläsionen angewendet wurde, ist der zugrundeliegende physikalisch-biologische Mechanismus des ESW-induzierten Biomineralisierungsprozesses noch unklar. Um die Biomineralisation-induzierende Wirkung von sich radiär ausbreitenden extrakorporalen Stoßwellen (rESW) und die Dosis-Wirkungs-Beziehung zu untersuchen, haben wir ein neu entwickeltes Tiermodell (Zebramuschel – Dreissena polymorpha) verwendet. Die aquatische Umgebung von Muscheln bietet ein homogenes Medium für die Übertragung von Stoßwellen und erlaubt eine feine Steuerung der Stoßwellenenergien und damit der Energiedosis, welche auf das Gewebe der Tiere einwirkt. Abgesehen von der Stoßwellen-induzierten Biomineralisation und ihrer Dosis-Wirkungs-Beziehung, ist der genaue biologische Mechanismus der die Muschelschalenmineralisierung antreibt noch unklar. Daher wurde auch eine immunhistochemische Studie zu Molekülen der extrazellulären Matrix (ECM) vorgenommen, um das Vorliegen potentiell mineralisationsbezogener Target Moleküle im Weichgewebe von Zebramuscheln zu demonstrieren.

In der ersten Studie wurden Zebramuscheln rESW in verschiedenen Energieniveaus ausgesetzt, gefolgt von der Analyse der Fluoreszenzintensität in den Wachstumsregionen der Schalen, jeweils getrennt nach Regionen sowohl in der linken als auch in der rechten Schalenhälfte. Im Vergleich zu den Kontrollgruppen zeigten die Muscheln, die unterschiedlichen Energien von rESWs ausgesetzt waren, in einigen Regionen eine signifikant höhere Fluoreszenzintensität, welche als Indikator für Mineralisationsvorgänge dient. Die Exposition von Muscheln in rESW wiederholte dabei im Wesentlichen die Ergebnisse bei Exposition in fokussierten ESW. In beiden Fällen wurden Anzeichen für eine Induktion zusätzlicher Mineralisation in Zebramuscheln beobachtet. Die Ergebnisse von Muscheln, die rESWT ausgesetzt waren, zeigen, dass rESWT eine neue Mineralisierung in Schalen induzieren kann. Außerdem zeigten die Ergebnisse, dass die durch rESWT induzierte Biomineralisation mit steigender Stoßwellenenergie zunimmt.

Der statistische Vergleich zwischen den Gruppen zeigte, dass es signifikante Unterschiede zwischen der Fluoreszenzintensität zwischen Gruppen mit unterschiedlichen Energieniveaus gibt. All diese Ergebnisse deuten darauf hin, dass rESWT dosisabhängige biomineralisationsinduzierende Wirkungen aufweist und dass mit zunehmender Biomineralisation nach Stoßwellen mit höherer Energie zu rechnen ist.

In einer zweiten Studie wurde ein immunhistochemischer Nachweis extrazellulärer Matrixbestandteile im Weichteilgewebe von Zebramuscheln durchgeführt. Die Ergebnisse bezüglich der Expression von Typ-IV-Kollagen, Fibronektin und Keratansulfat in Zebramuschel-Hämozyten stimmen unerwartet gut mit der sogenannten „Hämozyten-vermittelten“ Schalenbildungshypothese überein. Die Funktionen von Typ-IV-Kollagen, Fibronektin und Keratansulfat in Hämozyten würden demnach mit der Hämozyten-vermittelten Biomineralisierung zusammenhängen. Außerdem wurde Typ-IV-Kollagen auch im peripheren Nervensystem mit einer möglichen Rolle als Bestandteil der Basalmembran (Basallamina) beobachtet. Darüber hinaus wurde Aggrecan- und Link-Protein-Expression in verschiedenen Byssus-Drüsenzellen nachgewiesen. In Säugetiergeweben tragen Aggrecan und Link-Protein zur strukturellen Stabilität und Widerstandsfähigkeit gegen Druckkräfte bei. Das Aggrecan- und Link-Protein in den Drüsen des Muschel-Byssus Systems vorkommen, legt nahe, dass sie an der Synthese von Byssus-Fäden beteiligt sein könnten oder zumindest zur strukturellen Stärke der Byssus-Muskel-Verbindung beitragen. Darüber hinaus wurde festgestellt, dass einige extrazellulären Matrix-Komponenten (Laminin, Decorin und Osteonectin) in Zebramuschelgeweben weit verbreitet sind. Sie können eine Rolle bei der Gewebeorganisation spielen, indem sie die Biomineralisation verhindern, oder als Regulator der Mineralkristallbildung wirken. Diese in Weichgeweben von Zebramuscheln nachgewiesenen ECM-Moleküle von Säugetieren zeigen die Konservierung von bestimmten ECM-Molekülen in der Evolution des Lebens. Darüber hinaus liefern die Befunde unterstützende Argumente für die Hypothese der „Hämozyten-vermittelten“ Schalenbildung und dienen als Grundlage für weitere Untersuchungen von Zebramuscheln im Zusammenhang mit Biomineralisation.

7. References

1. Rosenberg G. A New Critical Estimate of Named Species-Level Diversity of the Recent Mollusca*. *American Malacological Bulletin.* **2014**;32:308. doi:10.4003/006.032.0204.
2. Vaughn CC. Ecosystem services provided by freshwater mussels. *Hydrobiologia.* **2018**;810:15-27. doi:10.1007/s10750-017-3139-x.
3. Harrington MJ, Jehle F, Priemel T. Mussel Byssus Structure-Function and Fabrication as Inspiration for Biotechnological Production of Advanced Materials. *Biotechnol J.* **2018**;13:e1800133. doi:10.1002/biot.201800133.
4. Lu M, Yu J. Mussel-Inspired Biomaterials for Cell and Tissue Engineering. *Adv Exp Med Biol.* **2018**;1077:451-74. doi:10.1007/978-981-13-0947-2_24.
5. Hartmann JT, Beggel S, Auerswald K, Stoeckle BC, Geist J. Establishing mussel behavior as a biomarker in ecotoxicology. *Aquat Toxicol.* **2016**;170:279-88. doi:10.1016/j.aquatox.2015.06.014.
6. Li J, Lusher AL, Rotchell JM, Deudero S, Turra A, Bråte ILN, et al. Using mussel as a global bioindicator of coastal microplastic pollution. *Environ Pollut.* **2019**;244:522-33. doi:10.1016/j.envpol.2018.10.032.
7. Lummer E-M, Auerswald K, Geist J. Fine sediment as environmental stressor affecting freshwater mussel behavior and ecosystem services. *Sci Total Environ.* **2016**;571:1340-8. doi:10.1016/j.scitotenv.2016.07.027.
8. Zuykov M, Pelletier E, Harper DAT. Bivalve mollusks in metal pollution studies: from bioaccumulation to biomonitoring. *Chemosphere.* **2013**;93:201-8. doi:10.1016/j.chemosphere.2013.05.001.
9. Marin F, Le Roy N, Marie B. The formation and mineralization of mollusk shell. *Front Biosci (Schol Ed).* **2012**;4:1099-125. doi:10.2741/s321.
10. Böhm CF, Harris J, Schodder PI, Wolf SE. Bioinspired Materials: From Living Systems to New Concepts in Materials Chemistry. *Materials (Basel).* **2019**;12(13):2117. doi:10.3390/ma12132117.
11. Song X, Liu Z, Wang L, Song L. Recent Advances of Shell Matrix Proteins and Cellular Orchestration in Marine Molluscan Shell Biomineralization. *Front. Mar. Sci.* **2019**;6:41. doi:10.3389/fmars.2019.00041.
12. Sternecker K, Geist J, Beggel S, Dietz-Laursonn K, La Fuente M de, Frank H-G, et al. Exposure of zebra mussels to extracorporeal shock waves demonstrates formation of new mineralized tissue inside and outside the focus zone. *Biol Open.* **2018**;7:bio033258. doi:10.1242/bio.033258.
13. Schmitz C, Császár NBM, Rompe J-D, Chaves H, Furia JP. Treatment of chronic plantar fasciopathy with extracorporeal shock waves (review). *J Orthop Surg Res.* **2013**;8:31. doi:10.1186/1749-799X-8-31.
14. Császár NBM, Angstman NB, Milz S, Sprecher CM, Kobel P, Farhat M, et al. Radial Shock Wave Devices Generate Cavitation. *PLoS One.* **2015**;10:e0140541. doi:10.1371/journal.pone.0140541.

15. Rassweiler JJ, Knoll T, Köhrmann K-U, McAteer JA, Lingeman JE, Cleveland RO, et al. Shock wave technology and application: an update. *Eur Urol.* **2011**;59:784-96. doi:10.1016/j.eururo.2011.02.033.

16. Salter CA, Lue TF, Mulhall JP. What Is Shockwave Therapy? *J Sex Med.* **2020**;17:565-9. doi:10.1016/j.jsxm.2020.01.004.

17. ISMST International Society for Medical Shockwave Treatment. Physical principles of ESWT: Basic physical principles. [Internet]. *ISMST - Shockwave Therapy.* **2018**. https://www.shockwavetherapy.org/about-eswt/physical-principles-of-eswt/. Accessed 24 Mar 2022.

18. Riesz P, Berdahl D, Christman CL. Free radical generation by ultrasound in aqueous and nonaqueous solutions. *Environ Health Perspect.* **1985**;64:233-52. doi:10.1289/ehp.8564233.

19. Ingber DE. Cellular mechanotransduction: putting all the pieces together again. *FASEB J.* **2006**;20:811-27. doi:10.1096/fj.05-5424rev.

20. Cheng J-H, Wang C-J. Biological mechanism of shockwave in bone. *Int J Surg.* **2015**;24:143-6. doi:10.1016/j.ijsu.2015.06.059.

21. Ha CH, Kim S, Chung J, An SH, Kwon K. Extracorporeal shock wave stimulates expression of the angiogenic genes via mechanosensory complex in endothelial cells: mimetic effect of fluid shear stress in endothelial cells. *Int J Cardiol.* **2013**;168:4168-77. doi:10.1016/j.ijcard.2013.07.112.

22. Holfeld J, Tepeköylü C, Kozaryn R, Urbschat A, Zacharowski K, Grimm M, Paulus P. Shock-wave therapy differentially stimulates endothelial cells: implications on the control of inflammation via toll-Like receptor 3. *Inflammation.* **2014**;37:65-70. doi:10.1007/s10753-013-9712-1.

23. Holfeld J, Tepeköylü C, Reissig C, Lobenwein D, Scheller B, Kirchmair E, et al. Toll-like receptor 3 signalling mediates angiogenic response upon shock wave treatment of ischaemic muscle. *Cardiovasc Res.* **2016**;109:331-43. doi:10.1093/cvr/cvv272.

24. Wang F-S, Wang C-J, Chen Y-J, Chang P-R, Huang Y-T, Sun Y-C, et al. Ras induction of superoxide activates ERK-dependent angiogenic transcription factor HIF-1alpha and VEGF-A expression in shock wave-stimulated osteoblasts. *J Biol Chem.* **2004**;279:10331-7. doi:10.1074/jbc.M308013200.

25. Weihs AM, Fuchs C, Teuschl AH, Hartinger J, Slezak P, Mittermayr R, et al. Shock wave treatment enhances cell proliferation and improves wound healing by ATP release-coupled extracellular signal-regulated kinase (ERK) activation. *J Biol Chem.* **2014**;289:27090-104. doi:10.1074/jbc.M114.580936.

26. Xu J, Chen H, Li X, Huang Z, Xu H, Yang H, Hu J. Optimal intensity shock wave promotes the adhesion and migration of rat osteoblasts via integrin β1-mediated expression of phosphorylated focal adhesion kinase. *J Biol Chem.* **2012**;287:26200-12. doi:10.1074/jbc.M112.349811.

27. Chen Y-J, Wurtz T, Wang C-J, Kuo Y-R, Yang KD, Huang H-C, Wang F-S. Recruitment of mesenchymal stem cells and expression of TGF-beta 1 and VEGF in the early stage of shock wave-promoted bone regeneration of segmental defect in rats. *J Orthop Res.* **2004**;22:526-34. doi:10.1016/j.orthres.2003.10.005.

28. Huang C, Holfeld J, Schaden W, Orgill D, Ogawa R. Mechanotherapy: revisiting physical therapy and recruiting mechanobiology for a new era in medicine. *Trends Mol Med.* **2013**;19:555-64. doi:10.1016/j.molmed.2013.05.005.

29. Wang C-J, Wang F-S, Yang KD. Biological effects of extracorporeal shockwave in bone healing: a study in rabbits. Arch Orthop Trauma Surg. 2008;128:879-84. doi:10.1007/s00402-008-0663-1.

30. Wang C-J, Wang F-S, Yang KD, Weng L-H, Hsu C-C, Huang C-S, Yang L-C. Shock wave therapy induces neovascularization at the tendon-bone junction. A study in rabbits. *J Orthop Res.* **2003**;21:984-9. doi:10.1016/S0736-0266(03)00104-9.

31. Martini L, Giavaresi G, Fini M, Torricelli P, Pretto M de, Schaden W, Giardino R. Effect of extracorporeal shock wave therapy on osteoblastlike cells. *Clin Orthop Relat Res.* **2003**;(413):269-80. doi:10.1097/01.blo.0000073344.50837.cd.

32. Klein-Nulend J, Bakker AD, Bacabac RG, Vatsa A, Weinbaum S. Mechanosensation and transduction in osteocytes. *Bone.* **2013**;54:182-90. doi:10.1016/j.bone.2012.10.013.

33. Takahashi K, Yamazaki M, Saisu T, Nakajima A, Shimizu S, Mitsuhashi S, Moriya H. Gene expression for extracellular matrix proteins in shockwave-induced osteogenesis in rats. *Calcif Tissue Int.* **2004**;74:187-93. doi:10.1007/s00223-003-0043-3.

34. Zhang H, Li Z-L, Yang F, Zhang Q, Su X-Z, Li J, et al. Radial shockwave treatment promotes human mesenchymal stem cell self-renewal and enhances cartilage healing. *Stem Cell Res Ther.* **2018**;9:54. doi:10.1186/s13287-018-0805-5.

35. Chaussy C, Schmiedt E, Jocham B, Brendel W, Forssmann B, Walther V. First Clinical Experience with Extracorporeally Induced Destruction of Kidney Stones by Shock Waves. *J Urol.* **1982**;127:417-20. doi:10.1016/S0022-5347(17)53841-0.

36. Schaden W, Mittermayr R, Haffner N, Smolen D, Gerdesmeyer L, Wang C-J. Extracorporeal shockwave therapy (ESWT)--First choice treatment of fracture non-unions? *Int J Surg.* **2015**;24:179-83. doi:10.1016/j.ijsu.2015.10.003.

37. Valchanou VD, Michailov P. High energy shock waves in the treatment of delayed and nonunion of fractures. *Int Orthop.* **1991**;15:181-4. doi:10.1007/BF00192289.

38. Willems A, van der Jagt OP, Meuffels DE. Extracorporeal Shock Wave Treatment for Delayed Union and Nonunion Fractures: A Systematic Review. *J Orthop Trauma.* **2019**;33:97-103. doi:10.1097/BOT.0000000000001361.

39. Koutalos A, Varitimidis S, Dailiana Z, Bargiotas K, Koutsogiannis A, Malizos KN. Operative management of humeral nonunions. Factors that influence the outcome. *Acta Orthop Belg.* **2015**;81:501-10.

40. Furia JP, Juliano PJ, Wade AM, Schaden W, Mittermayr R. Shock wave therapy compared with intramedullary screw fixation for nonunion of proximal fifth metatarsal metaphyseal-diaphyseal fractures. *J Bone Joint Surg Am.* **2010**;92:846-54. doi:10.2106/JBJS.I.00653.

41. Cacchio A, Giordano L, Colafarina O, Rompe JD, Tavernese E, Ioppolo F, et al. Extracorporeal shock-wave therapy compared with surgery for hypertrophic long-bone nonunions. *J Bone Joint Surg Am.* **2009**;91:2589-97. doi:10.2106/JBJS.H.00841.

42. Kertzman P, Császár NBM, Furia JP, Schmitz C. Radial extracorporeal shock wave therapy is efficient and safe in the treatment of fracture nonunions of superficial bones: a retrospective case series. *J Orthop Surg Res.* **2017**;12:164. doi:10.1186/s13018-017-0667-z.

43. Tischer T, Milz S, Weiler C, Pautke C, Hausdorf J, Schmitz C, Maier M. Dose-dependent new bone formation by extracorporeal shock wave application on the intact femur of rabbits. *Eur Surg Res.* **2008**;41:44-53. doi:10.1159/000128279.

44. Gollwitzer H, Gloeck T, Roessner M, Langer R, Horn C, Gerdesmeyer L, Diehl P. Radial extracorporeal shock wave therapy (rESWT) induces new bone formation in vivo: results of an animal study in rabbits. *Ultrasound Med Biol.* **2013**;39:126-33. doi:10.1016/j.ultrasmedbio.2012.08.026.

45. Schnurrer-Luke-Vrbanić T, Avancini-Dobrović V, Sosa I, Cvijanovic O, Bobinac D. Effect of radial shock wave therapy on long bone fracture repair. *J Biol Regul Homeost Agents.* **2018**;32:875-9.

46. Ramesh S, Zaman F, Madhuri V, Sävendahl L. Radial Extracorporeal Shock Wave Treatment Promotes Bone Growth and Chondrogenesis in Cultured Fetal Rat Metatarsal Bones. *Clin Orthop Relat Res.* **2020**;478:668-78. doi:10.1097/CORR.0000000000001056.

47. Frantz C, Stewart KM, Weaver VM. The extracellular matrix at a glance. *J Cell Sci*. **2010**;123:4195-200. doi:10.1242/jcs.023820.

48. Ozbek S, Balasubramanian PG, Chiquet-Ehrismann R, Tucker RP, Adams JC. The evolution of extracellular matrix. *Mol Biol Cell.* **2010**;21:4300-5. doi:10.1091/mbc.e10-03-0251.

49. Tanzer ML. Current concepts of extracellular matrix. *J Orthop Sci.* **2006**;11:326-31. doi:10.1007/s00776-006-1012-2.

50. Dyachuk V. Extracellular Matrix Components in Bivalvia: Shell and ECM Components in Developmental and Adult Tissues. *Fish Aquac J.* **2018**;9:2. doi:10.4172/2150-3508.1000248.

51. Brown NH. Extracellular matrix in development: insights from mechanisms conserved between invertebrates and vertebrates. *Cold Spring Harb Perspect Biol.* **2011**;3(12):a005082. doi:10.1101/cshperspect.a005082.

52. Gelse K, Pöschl E, Aigner T. Collagens--structure, function, and biosynthesis. *Adv Drug Deliv Rev*. **2003**;55:1531-46. doi:10.1016/j.addr.2003.08.002.

53. Ricard-Blum S. The collagen family. *Cold Spring Harb Perspect Biol*. **2011**;3:a004978. doi:10.1101/cshperspect.a004978.

54. Kjellén L, Lindahl U. Proteoglycans: structures and interactions. *Annu Rev Biochem.* **1991**;60:443-75. doi:10.1146/annurev.bi.60.070191.002303.

55. Carrino DA, Dennis JE, Wu TM, Arias JL, Fernandez MS, Rodriguez JP, et al. The avian eggshell extracellular matrix as a model for biomineralization. *Connect Tissue Res.* **1996**;35:325-9. doi:10.3109/03008209609029207.

56. Rosset EM, Bradshaw AD. SPARC/osteonectin in mineralized tissue. *Matrix Biol.* **2016**;52-54:78-87. doi:10.1016/j.matbio.2016.02.001.

57. Si J, Wang C, Zhang D, Wang B, Zhou Y. Osteopontin in Bone Metabolism and Bone Diseases. *Med Sci Monit.* **2020**;26:e919159. doi:10.12659/MSM.919159.

58. Moursi AM, Damsky CH, Lull J, Zimmerman D, Doty SB, Aota S, Globus RK. Fibronectin regulates calvarial osteoblast differentiation. *Journal of Cell Science.* **1996**;109:1369-80. doi:10.1242/jcs.109.6.1369.

59. Addadi L, Joester D, Nudelman F, Weiner S. Mollusk shell formation: a source of new concepts for understanding biomineralization processes. *Chemistry.* **2006**;12:980-7. doi:10.1002/chem.200500980.

60. Addadi L, Moradian J, Shay E, Maroudas NG, Weiner S. A chemical model for the cooperation of sulfates and carboxylates in calcite crystal nucleation: Relevance to biomineralization. *Proc Natl Acad Sci U S A.* **1987**;84:2732-6. doi:10.1073/pnas.84.9.2732.

61. Sikes CS, Wheeler AP, Wierzbicki A, Mount AS, Dillaman RM. Nucleation and growth of calcite on native versus pyrolyzed oyster shell folia. *Biol Bull.* **2000**;198:50-66. doi:10.2307/1542803.

62. Mount AS, Wheeler AP, Paradkar RP, Snider D. Hemocyte-mediated shell mineralization in the eastern oyster. *Science.* **2004**;304:297-300. doi:10.1126/science.1090506.

63. Kong W, Li S, Xiang L, Xie L, Zhang R. Calcium carbonate mineralization mediated by in vitro cultured mantle cells from Pinctada fucata. *Biochem Biophys Res Commun.* **2015**;463:1053-8. doi:10.1016/j.bbrc.2015.06.057.

64. Huang J, Li S, Liu Y, Liu C, Xie L, Zhang R. Hemocytes in the extrapallial space of Pinctada fucata are involved in immunity and biomineralization. *Sci Rep.* **2018**;8:4657. doi:10.1038/s41598-018-22961-y.

65. Zhang G, Fang X, Guo X, Li L, Luo R, Xu F, et al. The oyster genome reveals stress adaptation and complexity of shell formation. *Nature.* **2012**;490:49-54. doi:10.1038/nature11413.

66. Johnstone MB, Ellis S, Mount AS. Visualization of shell matrix proteins in hemocytes and tissues of the Eastern oyster, Crassostrea virginica. *J Exp Zool B Mol Dev Evol.* **2008**;310:227-39. doi:10.1002/jez.b.21206.

67. Joubert C, Piquemal D, Marie B, Manchon L, Pierrat F, Zanella-Cléon I, et al. Transcriptome and proteome analysis of Pinctada margaritifera calcifying mantle and shell: focus on biomineralization. *BMC Genomics.* **2010**;11:613. doi:10.1186/1471-2164-11-613.

68. Yin T-C, Wang C-J, Yang KD, Wang F-S, Sun Y-C. Shockwaves enhance the osteogenetic gene expression in marrow stromal cells from hips with osteonecrosis. *Chang Gung Med J.* **2011**;34:367-74.

69. Boszczyk BM, Boszczyk AA, Boos W, Korge A, Mayer HM, Putz R, et al. An immunohistochemical study of the tissue bridging adult spondylolytic defects--the presence and significance of fibrocartilaginous entheses. *Eur Spine J.* **2006**;15:965-71. doi:10.1007/s00586-005-0986-3.

70. Chatuparisute P, Shinohara Y, Kirchhoff C, Fischer F, Milz S. Immunohistochemical composition of the human lunotriquetral interosseous ligament. *Appl Immunohistochem Mol Morphol.* **2012**;20:318-24. doi:10.1097/PAI.0b013e31822a8fb3.

71. Milz S, Neufang J, Higashiyama I, Putz R, Benjamin M. An immunohistochemical study of the extracellular matrix of the tarsal plate in the upper eyelid in human beings. *J Anat.* **2005**;206:37-45. doi:10.1111/j.0021-8782.2005.00363.x.

72. Har-el R, Tanzer ML. Extracellular matrix. 3: Evolution of the extracellular matrix in invertebrates. *FASEB J.* **1993**;7:1115-23. doi:10.1096/fasebj.7.12.8375610.

73. Dyachuk V. Extracellular Matrix Components in Bivalvia: Shell and ECM Components in Developmental and Adult Tissues. *Fish Aquac J.* **2018**;9:2. doi:10.4172/2150-3508.1000248.

74. Corbetta S, Bairati A, Vitellaro Zuccarello L. Immunohistochemical study of subepidermal connective of molluscan integument. *Eur J Histochem.* **2002**;46:259-72. doi:10.4081/1688.

75. Evariste L, Auffret M, Audonnet S, Geffard A, David E, Brousseau P, et al. Functional features of hemocyte subpopulations of the invasive mollusk species Dreissena polymorpha. *Fish Shellfish Immunol.* **2016**;56:144-54. doi:10.1016/j.fsi.2016.06.054.

76. Tame A, Yoshida T, Ohishi K, Maruyama T. Phagocytic activities of hemocytes from the deep-sea symbiotic mussels Bathymodiolus japonicus, B. platifrons, and B. septemdierum. *Fish Shellfish Immunol.* **2015**;45:146-56. doi:10.1016/j.fsi.2015.03.020.

77. Donaghy L, Lambert C, Choi K-S, Soudant P. Hemocytes of the carpet shell clam (Ruditapes decussatus) and the Manila clam (Ruditapes philippinarum): Current knowledge and future prospects. *Aquaculture.* **2009**;297:10-24. doi:10.1016/j.aquaculture.2009.09.003.

78. Rebelo MdF, Figueiredo EdS, Mariante RM, Nóbrega A, Barros CM de, Allodi S. New insights from the oyster Crassostrea rhizophorae on bivalve circulating hemocytes. *PLoS One.* **2013**;8:e57384. doi:10.1371/journal.pone.0057384.

79. Immel F, Broussard C, Catherinet B, Plasseraud L, Alcaraz G, Bundeleva I, Marin F. The Shell of the Invasive Bivalve Species Dreissena polymorpha: Biochemical, Elemental and Textural Investigations. *PLoS One.* **2016**;11:e0154264. doi:10.1371/journal.pone.0154264.

80. Ha YW, Son MJ, Yun KS, Kim YS. Relationship between eggshell strength and keratan sulfate of eggshell membranes. *Comp Biochem Physiol A Mol Integr Physiol.* **2007**;147:1109-15. doi:10.1016/j.cbpa.2007.03.022.

81. Caterson B, Melrose J. Keratan sulfate, a complex glycosaminoglycan with unique functional capability. *Glycobiology.* **2018**;28:182-206. doi:10.1093/glycob/cwy003.

82. Panara F, Di Rosa I, Fagotti A, Simoncelli F, Mangiabene C, Pipe RK, Pascolini R. Characterization and immunocytochemical localization of actin and fibronectin in haemocytes of the mussel Mytilus galloprovincialis. *Histochem J.* **1996**;28:123-31. doi:10.1007/BF02331417.

83. Dyachuk VA, Maiorova MA, Odintsova NA. Identification of β integrin-like- and fibronectin-like proteins in the bivalve mollusk Mytilus trossulus. *Dev Growth Differ.* **2015**;57:515-28. doi:10.1111/dgd.12234.

84. Li S, Liu Y, Liu C, Huang J, Zheng G, Xie L, Zhang R. Hemocytes participate in calcium carbonate crystal formation, transportation and shell regeneration in the pearl oyster Pinctada fucata. *Fish Shellfish Immunol.* **2016**;51:263-70. doi:10.1016/j.fsi.2016.02.027.

85. Huang J, Li S, Liu Y, Liu C, Xie L, Zhang R. Hemocytes in the extrapallial space of Pinctada fucata are involved in immunity and biomineralization. *Sci Rep.* **2018**;8:4657. doi:10.1038/s41598-018-22961-y.

86. Chernousov MA, Yu W-M, Chen Z-L, Carey DJ, Strickland S. Regulation of Schwann cell function by the extracellular matrix. *Glia.* **2008**;56:1498-507. doi:10.1002/glia.20740.

87. Chen P, Cescon M, Bonaldo P. The Role of Collagens in Peripheral Nerve Myelination and Function. *Mol Neurobiol.* **2015**;52:216-25. doi:10.1007/s12035-014-8862-y.

88. Kiani C, Chen L, Wu YJ, Yee AJ, Yang BB. Structure and function of aggrecan. *Cell Res.* **2002**;12:19-32. doi:10.1038/sj.cr.7290106.

89. Yoon JH, Halper J. Tendon proteoglycans: biochemistry and function. *J Musculoskelet Neuronal Interact.* **2005**;5:22-34.

90. Coyne KJ, Qin XX, Waite JH. Extensible collagen in mussel byssus: a natural block copolymer. *Science.* **1997**;277:1830-2. doi:10.1126/science.277.5333.1830.

91. Tamarin A. An ultrastructural study of byssus stem formation in Mytilus californianus. *J Morphol.* **1975**;145:151-77. doi:10.1002/jmor.1051450204.

92. Zuccarello LV. The collagen gland of Mytilus galloprovincialis: an ultrastructural and cytochemical study on secretory granules. *J Ultrastruct Res.* **1980**;73:135-47. doi:10.1016/s0022-5320(80)90119-7.

93. Golser A, Scheibel T. Routes towards Novel Collagen-Like Biomaterials. *Fibers.* **2018**;6:21. doi:10.3390/fib6020021.

94. Benjamin M, Kumai T, Milz S, Boszczyk B, Boszczyk A, Ralphs J. The skeletal attachment of tendons—tendon 'entheses'. *Comp Biochem Physiol A Mol Integr Physiol.* **2002**;133:931-45. doi:10.1016/s1095-6433(02)00138-1.

95. Aumailley M. The laminin family. *Cell Adh Migr.* **2013**;7:48-55. doi:10.4161/cam.22826.

96. Buraschi S, Neill T, Goyal A, Poluzzi C, Smythies J, Owens RT, et al. Decorin causes autophagy in endothelial cells via Peg3. *Proc Natl Acad Sci U S A.* **2013**;110:E2582-91. doi:10.1073/pnas.1305732110.

97. Järveläinen H, Sainio A, Wight TN. Pivotal role for decorin in angiogenesis. *Matrix Biol.* **2015**;43:15-26. doi:10.1016/j.matbio.2015.01.023.

98. Lennon DP, Carrino DA, Baber MA, Caplan AI. Generation of a Monoclonal Antibody Against Avian Small Dermatan Sulfate Proteoglycan: Immunolocalization and Tissue Distribution of PG-II (Decorin) in Embryonic Tissues. *Matrix.* **1991**;11:412-27. doi:10.1016/S0934-8832(11)80196-4.

99. Zhu Y-S, Gu Y, Jiang C, Chen L. Osteonectin regulates the extracellular matrix mineralization of osteoblasts through P38 signaling pathway. *J Cell Physiol.* **2020**;235:2220-31. doi:10.1002/jcp.29131.

100. Seppinen L, Pihlajaniemi T. The multiple functions of collagen XVIII in development and disease. *Matrix Biol.* **2011**;30:83-92. doi:10.1016/j.matbio.2010.11.001.

101. Bishnoi M, Jain A, Hurkat P, Jain SK. Chondroitin sulphate: a focus on osteoarthritis. *Glycoconj J.* **2016**;33:693-705. doi:10.1007/s10719-016-9665-3.

Acknowledgements

I am deeply indebted to my supervisor Professor Dr. Christoph Schmitz for his trust in me and giving me this wonderful opportunity to do my Ph.D. work. I appreciate his kind support in my hard times and his extensive professional guidance in scientific research and my career life.

I would like to express my deep gratitude to my co-supervisor, Prof. Dr. Stefan Milz, who taught me, helped me and gave me guidance in the whole process of scientific research. I appreciate his patience, encouragement, shared experiences, and sense of humor.

I am very grateful to Dr. Katharina Sternecker for her guidance, suggestions, and scientific support throughout my Ph.D. career, and I appreciate her meticulous academic attitude.

I would also like to give my thanks to Prof. Dr. Juergen Geist, Prof. Dr. Nicola Maffulli, Prof. Dr. Hans-Georg Frank, Dr. John P. Furia, and Dr. Sebastian Beggel for their academic and technical support, and I appreciate their impressive participation. My thanks also go to Fangfang Liu and Dr. Lukas Meindlhumer for their supportive work.

All my colleagues at the institute deserve my appreciation for being supportive during my work. Especially, I am thankful to Claudia Harbauer, Andrea Haderer, Beate Aschauer, Barbara Mosler, and Astrid Baltruschat for their technical assistance.

Special thanks go to the China Scholarship Council for the financial support.

Many thanks to my friends Zhiyuan Wu, Kun Dai, Yiqun Zhang, Lin Li, Yuyu Liang, Ping Li, and Aminaa Sanchin for the greatest joy of their company in Germany. Most importantly, I would like to thank my big family in China for their infinite love and support during my life. I miss you, my dear grandmother.

I believe that the experience of scientific research and daily life in Germany will become precious life-long memories and will give me long-term benefits in my life. After this dissertation, I shall start my academic career as a doctor and researcher in China.